Physics – Uspekhi **64** (7) 722 – 739 (2021)

INSTRUMENTS AND METHODS OF INVESTIGATION PACS numbers: **42.79. – e**, 42.79.Hp, 78.20.Ls

Broadband integrated optical modulators: achievements and prospects

V M Petrov, P M Agruzov, V V Lebedev, I V Il'ichev, A V Shamray

DOI: https://doi.org/10.3367/UFNe.2020.11.038871

Contents

Abstract. Broadband integrated optical modulators are key elements of modern optical information systems. The three main technological material platforms for their manufacture are considered: lithium niobate, III–V semiconductors, and silicon. Progress achieved in the development of integrated optical modulators is analyzed, and the main parameters of modulators obtained for various materials are compared with requirements for practical applications. Directions in the further development of the technology of modulators related to new problems in optical information systems are discussed.

Keywords: electro-optic effect, microwave integrated optical modulators

1. Introduction

The use of an optical carrier in modern information technologies [1] offers a variety of advantages and opens new functional possibilities for the coding, transfer, storage and processing of information flows. The most spectacular and commercially successful example of the application of optics in information technologies is undoubtedly fiber-optic communication links [2]. Fiber-optic networks, being the skeleton of modern telecommunication structures, are information systems extending over huge spatial scales and featuring an extremely high transmission capacity and data processing rate. The further development of optical information technologies is related to the reduction of spatial dimensions by retaining broadband. The development of data centers for data processing is assumed, which will be followed by the creation of optical connections between chips and, finally, optical connections inside chips and optical processors.

The key elements of optical information systems used to superimpose a broadband signal on an optical carrier are optical modulators. The development of these systems involving the use of broadband information signals, a reduction in dimensions, and an increase in the packing density of components requires the manufacture of these optical devices in an integrated form.

In this paper, we review in detail the state of the art and the main trends in the development of broadband integrated optical modulators. Our estimates and explanations presented here are based on our long-standing experience in the development of integrated optical modulators and optical information systems based on these modulators, and much of the data on integrated optical modulators on lithium niobate substrates considered in the paper is our own original results.

In Section 2, the main fields of applications of broadband integrated optical modulators are briefly discussed, and arguments are presented in favor of applications of the external modulation of optical signals. In Section 3, the

V M Petrov [(1,a)], **P M Agruzov** [(2,b)], **V V Lebedev** [(2,c)], **I V Il'ichev** [(2,d)], **A V Shamray** [(2,e)]
[(1)] ITMO University,
Kronverksky prosp. 49/A, 197101 St. Petersburg, Russian Federation
[(2)] Ioffe Institute,
ul. Politekhnicheskaya 26, 194021 St. Petersburg, Russian Federation
E-mail: [(a)] vikpetroff@mail.ru, [(b)] piotrag@mail.ioffe.ru,
[(c)] vladimir_l@mail.ru, [(d)] iiv@mail.ioffe.ru,
[(e)] achamrai@mail.ioffe.ru

Received 20 May 2020, revised 16 November 2020
Uspekhi Fizicheskikh Nauk **191** (7) 760 – 780 (2021)
Translated by M Sapozhnikov

three main material platforms for manufacturing integrated optical modulators — lithium niobate, III–V semiconductors, and silicon — are considered. These material platforms are compared from the point of view of physical effects used for modulation. The main optical frameworks of integrated optical modulators are discussed in Section 4. Section 5 is devoted to microwave electrodes. The operation principles of traveling-wave electrodes on which broadband modulation is based are explained, the main criteria for optimizing the construction of electrodes are considered, and their parameters are estimated. In Section 6, the main technical characteristics of modulators are determined, while the modern level of parameters achieved using material platforms is presented and compared with the requirements of various application fields. In conclusion, the generalization is presented and material platforms are finally compared. The most promising directions in the further development of broadband integrated optical modulators are pointed out.

2. Fields of applications and advantages of the broadband external modulation of optical signals

At present, optical modulators are mainly used in analog, digital, and quantum optical communications [3, 4]. Other applications of optical modulators include the transfer and processing of microwave signals, so-called microwave photonics [5, 6], and the processing of signals from precise fiber-optic detectors [7].

Optical modulators solve the problem of data input into a communication line or signal processing where coherent optical radiation is used as a carrier. To date, modulators operating in the wavelength range from 450 nm to 3.5 μm have been developed [8]; however, the most desired spectral range is the so-called telecommunication wavelength range from 1500 to 1600 nm, where optical silica fibers have minimal losses.

From the point of view of technical realization, optical modulators are divided into two classes: direct (internal) modulation devices and external modulators. Direct modulators simultaneously generate optical radiation and modulate one of its parameters. An example of a direct modulation device is a popular semiconductor laser diode with pump-current modulation [9]. Many optical communication systems with a bandwidth up to 10 GHz use namely the direct modulation of the pump current of a laser diode [10]. Internal modulation lasers can operate at higher frequencies up to 30 GHz [11]. The application of direct modulation has been restricted so far by the fact that direct-modulation lasers generate signals with a linear frequency modulation (so-called chirp) and can be used in systems with a relatively low dispersion–distance product [12]. However, the increasing use of principles of coherent reception [13] has made the dispersion problem in a communication line (optical fiber) secondary. The main problem with modern direct-modulation laser diodes is the impossibility of combining the high coherence and low phase noises with a broadband modulation in one device.

When external modulators are used, the generation of optical radiation and modulation of its parameters are separated, which allows the laser and modulation parameters to be optimized separately. In this case, modulator parameters such as the frequency bandwidth and the conversion efficiency (the modulator sensitivity to a modulating signal) can be optimized, and laser parameters such as the optical carrier and its coherence, stability, and noise can be separately optimized. In determining the outlook for development, we can conclude that probably external modulation will continue to dominate both in the fastest telecommunication systems and in analog systems imposing specific requirements for the transfer of signals with minimal distortion and additional noise.

3. Physical effects for the broadband modulation of optical signals and material platforms for manufacturing broadband modulators

At present, as a rule, four effects are used to control the propagation of light with the help of electric signals: the linear electro-optic effect (Pockels effect) [14], electro-absorption effects (the Franz–Keldysh effect and the quantum-size Stark effect) [15, 16]), and the plasma-dispersion effect (the dependence of the refractive index on the charge-carrier density) [17].

The first three effects are extremely fast (the response time is of the order of a few picoseconds). These effects are related to a change in the potential produced by bound electrons in a crystal. The operation rate of modulators based on these effects is restricted by technologies rather than the rate of the effects themselves. The plasma-dispersion effect depends on the residence time of charge carriers in the optical waveguide. The rate of this effect is restricted by the mobility of charge carriers, and, for reasonable amplitudes of a modulating signal, the minimal response time is fractions of a nanosecond [17].

3.1 Electro-optic modulators based on lithium niobate

The fundamentals of using the linear electro-optic Pockels effect in broadband optical modulators are considered in detail in [3, 4, 17–19]. Integrated electro-optic modulators are manufactured of lithium niobate ($LiNbO_3$). A lithium niobate crystal is a ferroelectric without an inversion center and with a comparatively large intrinsic polarization along the z-axis belonging to the 3m crystallographic group [20]. Because the wavelength dependence of optical properties is rather weak in the wavelength range used in optical telecommunication systems, lithium niobate modulators are very convenient for WDM (Wavelength Division Multiplexing) optical telecommunication systems. The main electro-optic coefficient of modulators is $r_{33} \approx 30.8$ pm V^{-1}. The change in the refractive index caused by the Pockels effect is described by the linear expression

$$\Delta n_{z,\,\mathrm{LiNbO_3}} \approx n_\mathrm{e} - \frac{1}{2} n_\mathrm{e}^3 r_{33} E_z \,. \tag{1}$$

Here, n_e is the refractive index for an extraordinary wave, and E_z is the electric field applied along the z-axis. The applied field has no effect on the absorption of a material in the optical range.

The unique characteristics of lithium niobate [21] made it the 'gold standard' in the field of modulation of optical signals. The well-developed technology of growing lithium niobate crystals provides the production of single-crystal substrates (wafers) of high optical quality with a diameter above 100 mm. Lithium niobate has very low optical losses in the telecommunication wavelength range and, although its electro-optic characteristics are not so high, the crystal is low-sensitive to external actions and has stable characteristics

almost invariable in time in a broad range of temperatures and powers of optical and electric signals. A variety of technological solutions was proposed for manufacturing optical waveguides based on lithium niobate [22]. The most popular industrial technologies for manufacturing waveguides on lithium niobate substrates are the thermal diffusion of titanium [23] and low-temperature proton exchange followed by annealing [24].

Apart from the electro-optic effect, a variety of other effects is also inherent in lithium niobate, such as the piezoelectric and acousto-optic, pyroelectric, and nonlinear second-order effects, and the photorefractive effect, which can be used to manufacture complex integrated optical devices on lithium niobate substrates. At the same time, these effects can produce a parasitic influence, which should be minimized in integrated electro-optic modulators. The photorefractive and nonlinear effects restrict the maximum admissible power of optical radiation and the spectral range of optical signals. The photorefractive sensitivity decreases upon increasing the wavelength and proves to be insignificant in the telecommunication range at wavelengths of 1550 nm [25], but becomes noticeable at wavelengths below 1000 nm [26]. The piezoelectric and acousto-optic effects produce parasitic frequency-dependent modulation. Acoustic effects are a problem mainly at frequencies lower than 1 GHz and in analog applications [27, 28]. For many of the problems mentioned above, efficient technological solutions have been found, some problems being solved with the help of feedback electronic control systems [29].

The main competitors of lithium niobate as a basic material for integrated electro-optical modulators are electro-optic polymers [30]. Polymer integrated optical modulators have been extensively developed over the last 20 years. Polymers considerably exceed lithium niobate by their electro-optic characteristics, their electro-optic coefficient reaching 1600 pm V^{-1} [31]. However, problems related to temporal degradation and instability to high optical radiation powers prevent wide applications of integrated optical devices based on electro-optic polymers.

Investigations directed at the development of modulators based on lithium niobate were initiated back in the 1960s. The first optical waveguides on lithium niobate substrates manufactured by the method of reverse diffusion of lithium and integrated optical modulators based on them appeared early in the 1970s [32, 33]. From the end of the 1970s to the end of the 1980s, the development of modulators on $LiNbO_3$ substrates was focused on the problem of high-speed modulation in optical telecommunication lines [34–41] and the creation of optical switches [42–52]. The main focus was on the minimization of optical losses and optimization of the technology of manufacturing optical waveguides (first of all by the thermal diffusion of titanium) [48–50], as well as matching with a fiber-optic line and reducing radiation coupling and decoupling losses [51–54]. At the end of the 1980s, modulators based on lithium niobate became the key elements of fiber-optic communication systems [55, 56]. Various configurations of modulators with matched traveling-wave microwave electrodes were developed [57–63]. Recently, a modulation bandwidth reaching 300 GHz was demonstrated in experiments [64]. Considerable progress has been achieved in the improvement of the stability and reliability of modulators based on lithium niobate, the refinement of the packaging technique and coupling with an optical fiber, and the suppression and compensation of the temperature [65–67] and electric (direct current, DC) drift [68–72]. After 2000, with the advent of new modulation formats in optical telecommunication lines, modulators for their realization were also developed based on lithium niobate [73, 74]. Modulators using the quadrature phase shift keying (QPSK) [75] are at present the most widespread product in the field of integrated optics on lithium niobate substrates.

The further development of modulators based on lithium niobate is related to the advent of new technologies, the creation of waveguides with a high difference of refractive indices based on thin-film lithium niobate, which allows the manufacture of optical layouts with sizes characteristic of semiconductor electronics and opens possibilities for creating hybrid optoelectronic layouts on silicon substrates [76–79].

3.2 Modulators based on electro-absorption effects in III–V semiconductors

The Franz–Keldysh effect and quantum-mechanical Stark effect observed in III–V semiconductors are electro-absorption effects. These effects are related to a change in the absorption spectrum caused by an applied external electric field due to the efficient narrowing of the band gap during the inclination of the boundaries of the band structure, the deformation of the wave functions of charge carriers, the displacement of discrete levels, and the spatial redistribution of carriers in a quantum well. This, in turn, causes an increase in the absorption of light with a photon energy slightly smaller than the band gap energy [80]. The dependence of absorption on the electric field strength has no simple analytic descriptions. The change in absorption results in a change in the refractive index according to Kramers–Kronig relations [81] (the electrorefraction effect), which can be used for phase modulation or creating amplitude modulators based on a Mach–Zehnder interferometer. The dependence of the refractive index on an external electric field is close to quadratic [82]:

$$\Delta n_{\mathrm{InP}} \approx aE^b\,, \tag{2}$$

where a and b are empirically obtained coefficients; for indium phosphide, $a = 10^{-13}$ and $b = 1.6$ at a wavelength of 1550 nm.

Modern devices for the telecommunication wavelength range are based on heterostructures consisting of a set of multiple quantum wells (MQWs) formed by InGaAsP layers separated by barrier indium phosphide (InP) layers placed between n- and p-contact layers [83]. Note that, to increase the efficiency, modulators of this type operate at wavelengths close to the resonance transition. In this case, the change in the refractive index is much greater than in the modulators based on lithium niobate considered above. However, the increased efficiency of the phase modulation is inevitably related to achieving considerable optical absorption, as a rule, a few dB cm^{-1} (Fig. 1).

The high modulation efficiency allows building devices considerably shorter than modulators based on lithium niobate, and therefore total losses remain comparable ($\sim 3-5$ dB). However, while optical losses in modulators based on lithium niobate are mainly related to scattering and do not result in heat release, a considerable portion of optical losses in MQW modulators is caused by light absorption resulting in device heating, thereby restricting the maximum optical power. This can be important in analog systems of microwave photonics, where the increase in the transmission

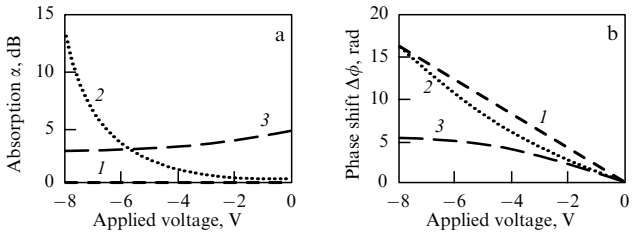

Figure 1. Dependences of absorption (a) and phase shift (b) on the applied voltage for an ideal modulator and typical InP and Si phase modulators 5 mm in length. (*1*) ideal modulator, (*2*) InP modulator, (*3*) Si modulator.

coefficient and the expansion of the dynamic range are achieved by increasing the optical power to 100 mW and above.

A strong wavelength dependence of the modulation efficiency complicates applications of MQW modulators for multichannel operation with optical radiation at different wavelengths. The disadvantages mentioned above also result in additional noise, depending on the characteristics of the optical radiation. As a result, MQW modulators are considerably inferior to those based on lithium niobate in practical applications sensitive to the noise level, such as microwave photonics and quantum communication systems. The sensitivity of MQW modulators to temperature variations in the environment can be reduced by stabilizing the temperature of modulators using Peltier elements.

The obvious advantage of modulators based on III–V semiconductors is their small size and the possibility of integrating them with other optoelectronic elements such as lasers and photodetectors manufactured on the same technological platform.

3.3 Silicon modulators based on the plasma-dispersion effect

Silicon is widely used for various applications in electronics. However, the absence of an efficient high-speed modulation mechanism for this material, unlike its competitors, gives rise to difficulties. Silicon would not be the best choice as a material for modulators if not for the possibility of integration with silicon electronic circuits [84].

The idea of using silicon was proposed long ago [85], but it became really attractive only recently, which is related to the improvement in the technology of manufacturing waveguides with a resolution below 1 μm and the achievement of optical losses on Si/SiO_2 substrates smaller than 1 dB cm^{-1}. Silicon waveguides have large differences among refractive indices with respect to the substrate material ($n = 3.5$ for Si and $n = 1.45$ for SiO_2), which provides a small transverse size (~ 1 μm) and a small critical bend radius (down to 10 μm). A disadvantage is the restriction on the admissible power: two-photon absorption can cause problems even at powers of about a few mW at a wavelength of 1550 nm [86].

The linear electro-optic (EO) effect in silicon is impossible because of crystal symmetry. Quadratic and electro-acoustic (EA) effects are also very weak, and for this reason the modulation in silicon is performed using the plasma-dispersion effect related to a change in the density of charge carriers [87, 88]. Note that, due to the small transverse dimensions of silicon waveguides, strong electric fields can appear in silicon modulators at low voltages. The modulator structure is a p–n junction which is forward-biased for operating in the charge-injection regime or reverse-biased for charge separation. A change in the refractive index is related to the density of free charge carriers (plasma) and is described by an empirical expression which has the form [87, 89, 90]

$$\Delta n_{Si} \approx -8.8 \times 10^{-22}\Delta N_e - 8.5 \times 10^{-18}(\Delta N_h)^{0.8} \quad (3)$$

for a wavelength of 1550 nm, where ΔN_e and ΔN_h are changes in the electron and hole concentrations, respectively. A similar expression also exists for absorption, which increases with increasing concentration of charge carriers:

$$\Delta\alpha_{Si} \approx 8.5 \times 10^{-18}\Delta N_e + 6.0 \times 10^{-18}\Delta N_h\,. \quad (4)$$

The dependence of the concentration of free carriers on a voltage applied to the p–n junction is complicated. Moreover, the width of the spatial charge region and the modulation efficiency nonlinearly depend on the position of the operating point of the modulator.

An exact analytic expression for the nonlinear dependence of the refractive index for silicon modulators is difficult to obtain, as it is for modulators based on indium phosphide. Because of this, a polynomial approximation with empirically found coefficients is used as a rule. Note that silicon modulators have a lower efficiency than indium phosphide modulators and also have relatively high optical losses caused by absorption; however, the dependence of losses on the applied voltage is weaker (see Fig. 1). Note again that the plasma-dispersion effect is restricted in the modulation rate (1–10 ns), which depends on the residence time of charge carriers in the optical waveguide. These limits can be displaced by shortening the lifetime of carriers producing defects or operating in the depletion regime; however, this increases the switching voltage [91].

4. Classification of integrated optical modulators by their optical framework

We considered in Section 3 various physical mechanisms of modulation of optical signals for the high-speed control of the amplitude and phase of optical radiation. Phase control is energetically more advantageous, because the optical power is not reduced in this case; however, this control is more complicated, because coherent methods should be used for detection. In addition, other parameters of optical radiation can also be modulated, which can offer some advantages and open up additional functional possibilities. These parameters are the polarization and wavelength. Broadband phase modulation is transformed to the modulation of other parameters using various optical schemes. Some of them are considered in Sections 4.1–4.5 (Fig. 2).

4.1 Straight optical waveguide

The simplest optical scheme of a modulator contains a straight optical waveguide and a system of electrodes for applying an electric field to the waveguide (Fig. 3). Such a scheme is widely used in phase electro-optic lithium niobate modulators. A system of electrodes in the simplest case includes two planar metal film conductors parallel to the optical waveguide. Note that electro-optic modulators are manufactured from noncentrally symmetric materials and have anisotropic electric and optical properties. Therefore, electro-optic modulators are polarization-dependent devices. Thus, to achieve the maximum electro-optic coefficient r_{33} in the case of lithium niobate phase modulators, the polariza-

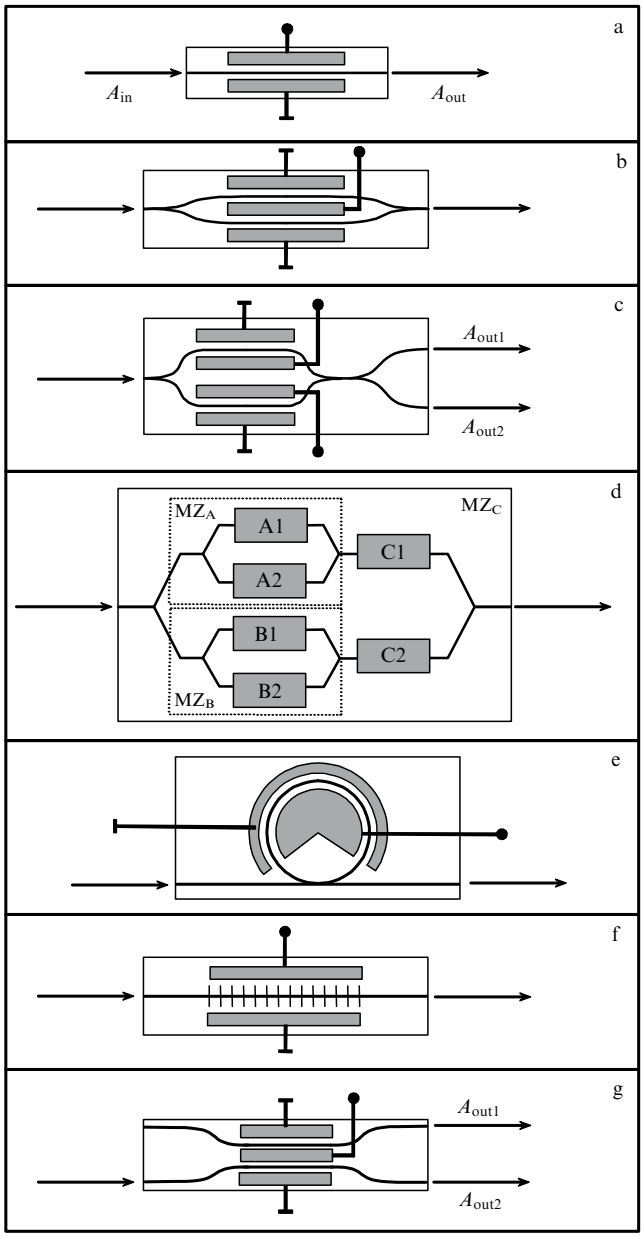

Figure 2. Main optical schemes of integrated optical modulators. (a) Single straight optical waveguide. (b) Mach–Zehnder (MZ) interferometer. (c) MZ interferometer with two outputs and two HF control inputs. (d) Composite modulator consisting of several MZ interferometers. (e) Resonance (ring) modulator. (f) Bragg grating modulator. (g) Controllable directional coupler.

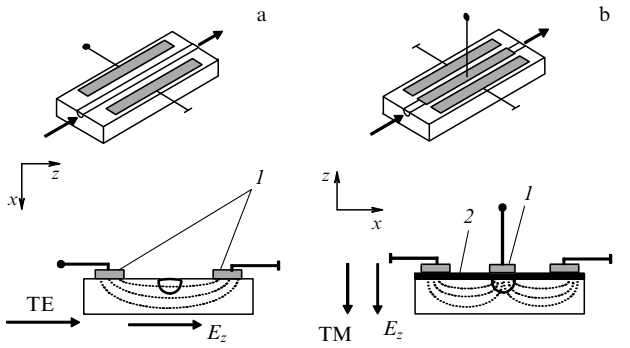

Figure 3. Two main configurations of phase modulators for efficient electro-optic modulation. (a) *X*-cut of a substrate; waveguide is located between electrodes, the field component and light polarization are parallel to the substrate plane. (b) *Z*-cut of a substrate; optical waveguide is located under an electrode, the field component and light polarization are normal to the substrate plane; a dielectric sublayer must be inserted between a metal electrode and an optical waveguide to reduce the absorption of light in the metal electrode. (*1*) electrodes, (*2*) dielectric sublayer.

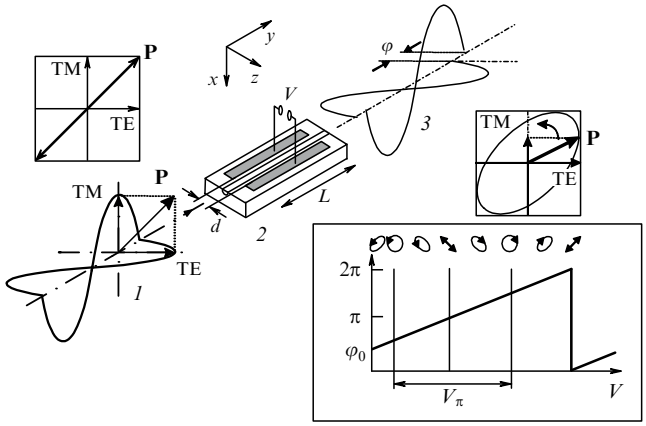

Figure 4. Modulation of polarization on an electrically controlled integrated optical phase plate. (*1*) input plane, (*2*) electrically controlled integrated optical phase plate, (*3*) input plane; L is the length of electrodes, d is the interelectrode gap. The inset at the bottom right shows the dependence of the phase modulation amplitude on the applied voltage; φ_0 is the initial phase difference, $\varphi_0 = (2\pi/\lambda)L(n_0 - n_e) - 2\pi N$, $N = 1, 2, 3\ldots$.

tion of light should be linear and directed along the electric field and the optical axis of a crystal. This determines the requirements for the relative orientation of the crystallographic axes of a substrate and the direction of light propagation in the optical waveguide.

Low-frequency integrated optical lithium niobate phase modulators (up to 300 MHz) are manufactured on *X*-cut substrates and use the transverse electric (TE) polarization of optical radiation and the electric-field component parallel to the substrate plane (see Fig. 3a). High-frequency phase modulators (> 1 GHz) are manufactured on *Z*-cut substrates and use the transverse magnetic (TM) polarization of optical radiation and the electric-field component perpendicular (Fig. 3b) to the substrate plane. In the first case, the optical waveguide is located in an interelectrode gap, while in the second case, under one of the electrodes. To prevent the absorption of TM-polarized light in a metal electrode, a buffer layer is used with the refractive index smaller than the refractive index of the substrate.

If a polarization mode different from the eigenmode is incident on an anisotropic phase modulator, the modulator operates as an electrically controlled phase plate (Fig. 4), i.e., it is transformed into a polarization modulator. A linear polarization oriented at an angle of 45° to the optical axis of a lithium niobate crystal is most often used. An external electric signal causes the modulation of the phase difference between two polarization eigenmodes, which results in the modulation of polarization states at the output (see Fig. 4):

$$\Delta\varphi = \frac{2\pi}{\lambda} L \left[(n_0 - n_e) - \frac{1}{2}(n_e^3 r_{33} - n_0^3 r_{13}) E_z \right]. \qquad (5)$$

For lithium niobate, $r_{33} = 30.8$ pm V^{-1} and $r_{13} = 8.6$ pm V^{-1} [92].

With the use of electro-absorption in III–V semiconductors, this scheme operates as an amplitude modulator. The

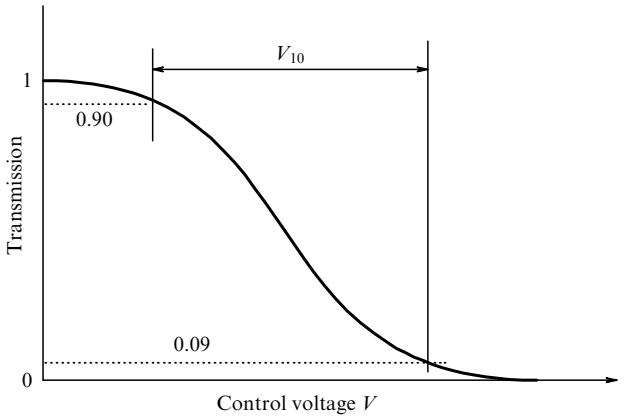

Figure 5. Transfer characteristic of an electroabsorption modulator. V_{10} is the voltage required to change transmission 10 times.

transfer function for this case is shown in Fig. 5. Such miniature devices (about a few hundred micrometers in size) are usually integrated together with a laser diode. They provide a change in absorption by more than 10 dB for an applied voltage of less than 2 V with the electric passband of more than 40 GHz [93], which is very important for most practical applications. The disadvantages of electro-absorption modulators (EAMs) are the appearance of a chirp due to the change in the refractive index, considerable heating because of operation at the absorption edge (which strongly restricts the optical power [94]), and the generation of a modulated current, which introduces additional noise and is an important critical factor for analog applications [95].

4.2 Mach–Zehnder interferometer

Figure 2b shows the optical scheme of one of today's most popular modulators based on a Mach–Zehnder interferometer [96] (Rozhdestvensky interferometer [14]), which is called a Mach–Zehnder modulator (MZM) in the modern literature [3, 4, 97]. Mach–Zehnder modulators are being developed on all key technological platforms: lithium niobate, III–V semiconductors, and silicon. Modulation is performed by producing a phase shift between the optical radiation in the individual interferometer arms. Depending on the relation of phases, either constructive interference (the transmitted light intensity is maximal) or destructive interference (the transmitted light intensity is close to zero) can be obtained at the output [97].

Figure 2c shows a modified MZM scheme, one with a so-called double high-frequency input and double optical output. A system of electrodes provides independent electro-optic modulation in different arms of the Mach–Zehnder interferometer. The interferometer output is made in the form of a directional coupler with the division coefficient of −3 dB. Such a setup is used to suppress laser noise during balance detection [98].

If the phase difference between the interferometer arms is produced using the linear EO effect, as, for example, in modulators on lithium niobate substrates, while the optical power in the arms is ideally divided in the ratio 1:1, the power transfer function of such a device is described by the cosine dependence (Fig. 6),

$$T = |E|^2 = \frac{1}{2}(1 + \cos\varphi)\,. \tag{6}$$

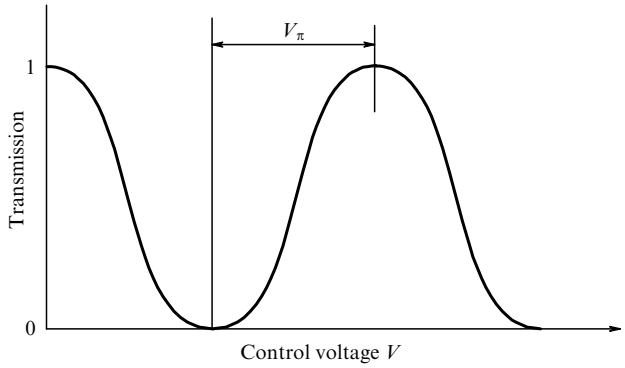

Figure 6. Transfer characteristic of MZM. V_π is the half-wave voltage.

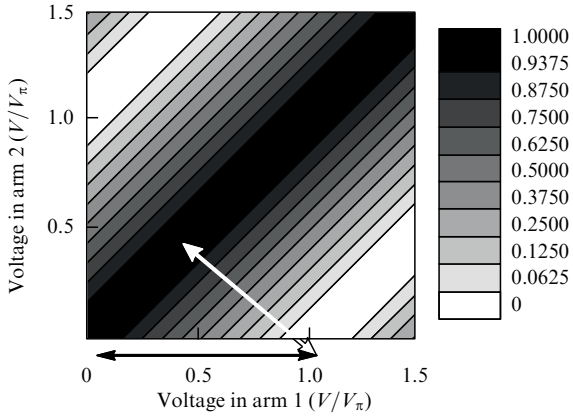

Figure 7. Contour plot of the dependence of the normalized optical power for a symmetric MZM doubly controlled by voltage in the arms.

Here, T is the optical transmission coefficient, E is the optical radiation amplitude, and φ is the phase difference between the interferometer arms. Expression (6) is valid for all MZMs independent of the effect used to produce the phase modulation.

For semiconductor modulators having a nonlinear response and additional modulation of absorption, the transfer function T has a more complicated form.

The output signal of an MZM can be written as

$$\begin{aligned} E(t) &= \frac{1}{2}\,E_0 \exp\left[\mathrm{i}\Delta\beta\big(V_1(t)\big)L\right] + \exp\left[\mathrm{i}\Delta\beta\big(V_2(t)\big)\right] \\ &= E_0 \cos\frac{\Delta\beta\big(V_2(t)\big) - \Delta\beta\big(V_1(t)\big)}{2} \\ &\times L \exp\left\{\mathrm{i}\left[\Delta\beta\big(V_2(t)\big) + \Delta\beta\big(V_1(t)\big)\right]L\right\}. \end{aligned} \tag{7}$$

Here, $\Delta\beta(V)$ is a change in the propagation constant, V_1 and V_2 are voltages in arms 1 and 2, and L is the interaction length of the modulator arms. In the case of the linear dependence of the phase on voltage, which is typical for electro-optic modulators, expression (7) takes the form

$$E(t) = \frac{E_0}{\sqrt{2}}\big(1 + \cos\varphi(t)\big)^{1/2} \exp\big(\mathrm{i}\varphi(t)\big)\,, \tag{8}$$

where $\varphi(t) = (\pi/V_\pi)(V_2(t) - V_1(t))$ is the phase difference between interferometer arms depending on the half-wave voltage V_π. The voltage switching the modulator from the $T = 1$ state to the $T = 0$ state is called the half-wave voltage. It corresponds to a voltage producing a phase shift of π between interferometer arms. By varying the voltage applied to each of the MZM arms, one can obtain a plot for the normalized output power (Fig. 7).

The black and white arrows in Fig. 7 indicate the operation conditions of MZMs most often used in practice both with the linear frequency modulation (chirp) and without it. If the MZM is made in a material with low losses in an optical waveguide (for example, $LiNbO_3$), the half-wave voltage can be reduced by increasing the interaction length.

4.3 Composite modulators

Composite modulators (Fig. 2d) are formed by a series, parallel, or more complicated combination of several modulators. Most often, MZM combinations with each other or other modulators are used. On the one hand, the advantage of such modulators is their wider functional possibilities. On the other hand, their substantial disadvantage is the much more strict requirements for the control system and a complicated manufacturing technology process.

An example is two (four) parallel MZMs with zero chirp in the arms of a Mach–Zehnder interferometer [99]. Such a modulator is used to modulate a carrier with one sideband [100]. The same scheme can be used to produce quadrature phase modulation and differential quadrature phase modulation [101] (Fig. 8). One modulator generates the in-phase component of a signal, while another, with the phase shift $\pi/2$, produces the quadrature component. Higher modulation levels can be achieved in a cascade of an MZM and a phase modulator [102].

The main reason for the development of composite modulators was linearization in analog communication systems [103] and the appearance of new modulation formats in digital lines. Here, we mention only a small part of all the models of such devices. Note that this area is being extensively developed at present and new designs of composite modulators are proposed for various practical applications.

4.4 Modulators based on optical filters

Some optical schemes of modulators are obtained from optical filters. The main idea is the shift of the transmission band of the filter by a small voltage change. If the light frequency lies at the boundary of the filter transmission band, a small change in the voltage will produce a change in the transmission coefficient. The modulation frequency band of such devices is usually restricted by the transmission band of the optical filter. Note that optical filters can be used not only for amplitude modulation but also for phase modulation because of a strong dispersion near the resonance wavelength [104].

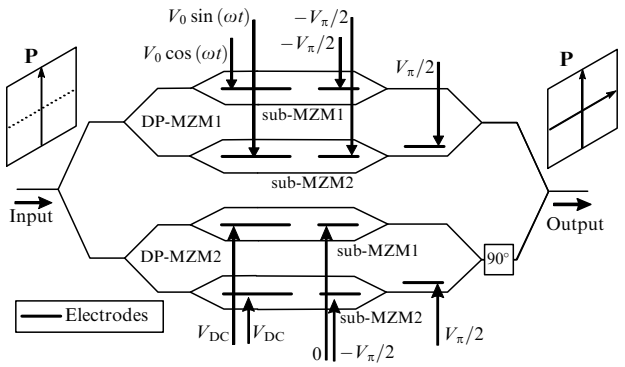

Figure 8. Diagram of a composite modulator and electric signals applied to it for producing the Differential Quadrature Phase Shift Keying (DQPSK). Dual-Parallel Mach–Zehnder Modulator (DP-MZM).

The spectral selectivity of modulators based on optical filters makes them especially convenient for obtaining the independent modulation of spectral channels in WDM (wavelength division multiplexing) systems. With the use of broadband optical radiation sources, modulators based on optical filters offer additional options for modulating the optical spectrum [105, 106], producing both a simple frequency shift coding and a more complicated control of the form of spectrum. Spectral modulation can be efficiently used as an additional service channel for transmitting control signals to remote devices of branched optical networks [107].

The most promising type of modulator based on optical filters are those in the form of optical ring resonators (Fig. 2e) based on silicon waveguides [108–110]. Due to their high quality (Q-factor) ($\sim 10^4 - 10^5$), providing a narrow spectral band of the optical filter, and their compact size (the typical diameter of a ring resonator is 10–20 μm), this type of modulator is characterized by a low control voltage (less than 0.5 V) and a high modulation rate (the typical switching time is a few ten picoseconds).

The simplest optical scheme of a modulator based on a ring resonator consists of a waveguide ring connected to a straight optical waveguide via a directional coupler (Fig. 9a). The intensity transmission coefficient of this structure is described by the expression [111, 112]

$$T_N = \frac{I_{\text{pass}}}{I_{\text{input}}} = \frac{a^2 - 2ra\cos\phi + r^2}{1 - 2ar\cos\phi + (ra)^2}\,, \tag{9}$$

where r is the coefficient of direct transfer of the amplitude of optical radiation by a directional coupler, which, together with the cross-transfer coefficient k, determines the optical power division $r^2 + k^2 = 1$, and $N = 1, 2, 3$ denote the critical, strong, and weak coupling regimes, respectively. The parameter $a^2 = \exp(-\alpha_{\text{opt}} L)$ describes optical losses in the resonator ring determined by the decay coefficient α_{opt} [m^{-1}] of a ring with length L, and $\phi = 2\pi L n_{\text{eff}}/\lambda$ is the phase incursion in the resonator ring formed by the optical waveguide with the effective refractive index n_{eff}. The resonance excitation wavelengths correspond to the condition $\lambda_{\text{m}} = n_{\text{eff}} L/m$. The simplest modulation method involves a change in the effective refractive index n_{eff} resulting in detuning from resonance conditions.

The transmission coefficient of an ideal resonator without losses $a = 1$; the transmission coefficient is unity for any phase incursion in the ring (for any detuning). Thus, the ideal resonator without losses cannot be used for amplitude modulation. However, in the region of resonances, the phase shift

$$\varphi = \pi + \phi + \arctan\frac{r\sin\phi}{a - \cos\phi} + \arctan\frac{ra\sin\phi}{1 - ra\cos\phi} \tag{10}$$

is observed, which can be used in principle for the phase modulation.

Figure 9b shows dependences T_N and φ calculated by expressions (9) and (10), respectively. The extinction ER_N for each of the coupling regimes was determined from the expressions

$$\text{ER}_N = 101g\left(\frac{T_{\max N}}{R_{\min}}\right), \tag{11a}$$

$$T_{\max N} = \frac{(r+a)^2}{(1+ra)^2}\,, \quad R_{\min N} = \frac{(r-a)^2}{(1-ra)^2}\,. \tag{11b}$$

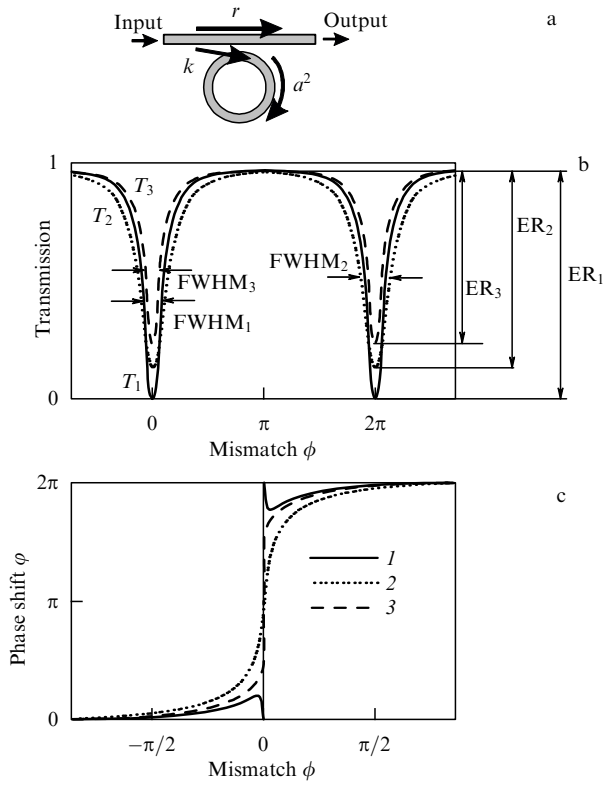

Figure 9. (a) Optical scheme of the simplest ring resonator in the all-pass configuration, r is the coefficient of direct transfer of the amplitude of optical radiation by a directional coupler, k is the cross-transfer coefficient, a^2 is a parameter describing optical losses. (b) Dependence of the optical transmission T of a ring resonator on the phase mismatch φ for different coupling regimes. T_1: the critical coupling regime ($r = a$), T_2: the strong coupling regime (above critical) ($r < a$), T_3: the strong coupling regime (below critical) ($r > a$), FWHM: full width of a band at half-maximum, ER$_N$: extinction ratio. (c) Dependence of the phase shift φ on the detuning ϕ in the critical coupling (*1*), strong coupling (*2*), and weak coupling (*3*) regimes.

The most interesting case from a practical point of view is that of the critical coupling $r = a$: the transfer coefficient at the resonance wavelength decreases to zero and the phase experiences a jump by 2π (Figs 9b, c). This regime provides the maximum contrast of the amplitude and phase modulation (Figs 10, 11). Therefore, the design of modulators is chosen to provide conditions close to the critical coupling conditions.

An increase in the coefficient r transforms the ring resonator into the weak-coupling state, the width of the resonance peak narrows, the amplitude drops, and the phase shift in the resonance region decreases (Figs 9b, c). As the coefficient r decreases, the ring resonator moves to the strong-coupling state, the resonance peak broadens, the amplitude drop decreases, and the phase jump in the resonance region is smoothed. Different spectral characteristics for different coupling states lead to different dynamics of the variations of the amplitude and phase of a modulated optical signal, which should be taken into account in the use of modulators based on ring resonators [113].

The limiting contrast of the amplitude modulation depends on how far the resonator state is from the ideal critical-coupling state.

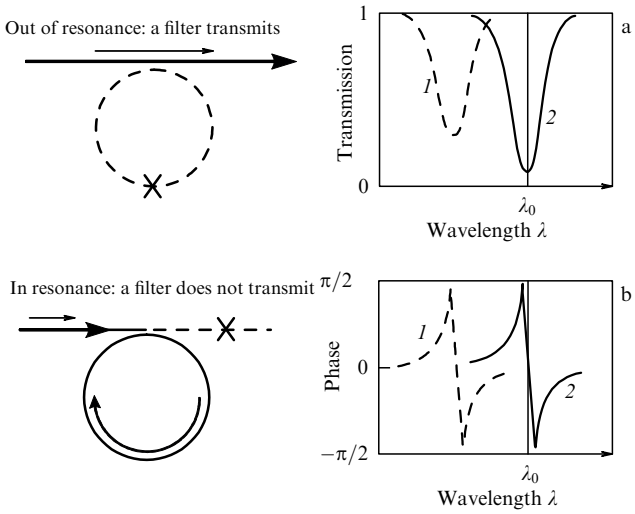

Figure 10. Modulation upon shifting the frequency band of an optical filter by the example of a ring resonator with nearly critical coupling between the ring and waveguide. λ_0 is the laser wavelength, *1* is 'out of resonance' state, $V = 0$, *2* is 'in resonance' state, $V = V_0$.

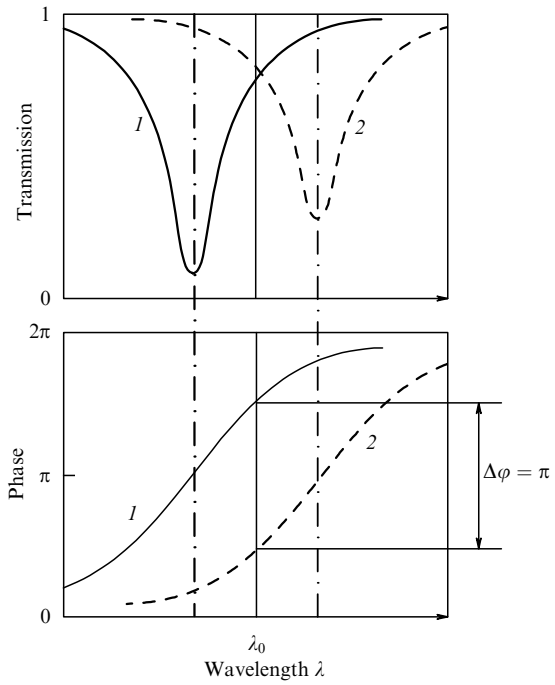

Figure 11. Phase coding using a ring resonator with an above-critical coupling. Wavelength dependences of the transmission and phase for the two states of a filter. λ_0 is the laser wavelength, *1* and *2* are filter states.

Spectral selective properties of a ring resonator are characterized by the following parameters [111, 112]:

$$\mathrm{FWHM} = \frac{(1 - ra)\lambda_{\mathrm{res}}^2}{\pi n_{\mathrm{g}} L \sqrt{ra}}\,, \tag{12}$$

$$\mathrm{FSR} = \frac{\lambda^2}{n_{\mathrm{g}} L}\,. \tag{13}$$

Note that both the FWHM (Full Width at Half-Maximum) of the resonance peak and the spectral distance between resonance peaks FSR (Free Spectral Range) depend on the

group refractive index characterizing the group velocity dispersion of the waveguide:

$$n_g = n_{eff} - \lambda_0 \frac{dn_{eff}}{d\lambda} . \quad (14)$$

The Q-factor of the resonator is determined by losses in the ring and the coupling coefficient of the directional coupler:

$$Q = \frac{\lambda_{res}}{FWHM} = \frac{\pi n_g L \sqrt{ra}}{\lambda_{res}(1-ra)} . \quad (15)$$

The modern technological level of manufacturing silicon waveguides provides $Q \sim 10^5$ [114]. The modulation is normally performed using the shift of the resonance wavelength with changing effective refractive index of the ring resonator, a great advantage of high-Q resonance modulators being the fact that the modulation efficiency increases with the Q-factor of the resonator. However, the modulation rate (the switching time) is directly related to the lifetime of photons in the resonator, which increases with increasing Q-factor ($\tau \approx Q\lambda/(2\pi c)$). For this reason, the design of modulators is based on a compromise, and the Q-factor is commonly made no higher than $Q = 10^4$, corresponding to the photon lifetime in the resonator $\tau \approx 8$ ps.

The modulation of the coupling coefficient of a directional coupler [115] allows one to overcome the rate limit restricted by the photon lifetime in the resonator ring [116]. A change in the coupling coefficient near the critical-coupling conditions results in a change in the optical transmission coefficient. However, efficiently controlling the coupling coefficient is quite complicated in practice because of the small interaction length in a directional coupler. The modulator uses more complex coupling devices, such as a Mach–Zehnder interferometer (Fig. 12) [117]. Another problem is that the optical power in the resonator gradually decays with deviation from critical-coupling conditions, which leads to the growth of distortions. To solve this problem, special optical schemes were proposed with an additional optical input for maintaining a constant power in the resonator [118] or with additional ring resonators [119]. Although theoretical models predict in fact the unlimited frequency band of resonance ring modulators based on coupling-coefficient modulation, at present, the broadening of the modulation band up to 30–40 GHz has been demonstrated in experiments [120], which is comparable to the results obtained for the best devices using the wavelength shift.

Figure 13a shows a silicon ring modulator with the modulated shift of the resonance wavelength based on the plasma dispersion effect (the main mechanism of the refractive index control in silicon waveguides) [121]. A ring resonator based on ridge waveguides is made in the silicon-on-insulator (SOI) configuration. The characteristic width W of waveguides is about 400 nm, while the gap width g in a directed coupler between a straight and ring waveguide is 200 nm in this case. The ring diameter is $D = 12$ μm. A small ring diameter allows this modulator to be considered a lumped-electrode for modulating microwave signals. In addition, the small area makes modulators based on silicon ring resonators very efficient from the point of view of the modulating signal energy required for the transfer of one information bit [115]. It is possible to modify modulator electrodes to an electric resonator microwave structure, which further increases the modulation efficiency [122, 123] but narrows the modulation band.

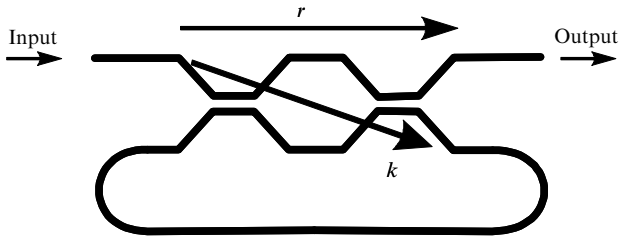

Figure 12. Optical schematic of a modulator based on a ring resonator with the modulated coupling coefficient in which a directional coupler is replaced by a Mach–Zehnder interferometer [116].

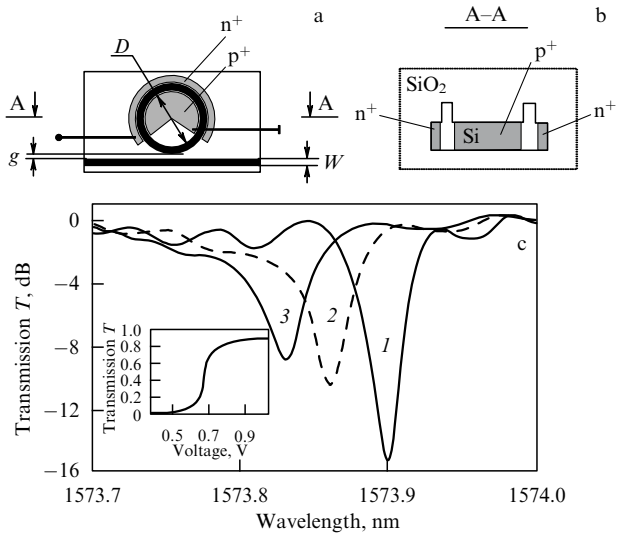

Figure 13. (a) Modulator based on a ring microresonator. W is the width of a straight waveguide, g is the gap between the straight waveguide and the ring resonator, D is the ring diameter. (b) Transverse section along A–A. (c) Shift of the spectral characteristic upon a forward biasing and the amplitude transfer characteristic of the modulator [121].

An optical waveguide in the active part of the ring is made in the form of a p–i–n-diode. This configuration provides the most efficient modulation of the refractive index due to the accumulation of charge carries. A forward bias applied to the p–i–n-diode causes a considerable increase in the concentration of charge carriers in the waveguide, which results in a blue shift of the resonance peak (Fig. 13c). Note that the shift is accompanied by an increase in losses and reduction in the Q-factor, thereby breaking the critical-coupling conditions for the resonator and decreasing the modulation contrast. The typical contrast of the amplitude modulation for silicon modulators based on ring resonators does not exceed 15–20 dB.

The modulator speed is determined by three time constants: the photon lifetime in the resonator, which is determined, as mentioned, by the Q-factor, the injection time of charge carriers with the forward bias of the p–i–n-diode, and the time of removing carriers from the optical waveguide with the reverse bias.

The characteristic time required for injecting carriers into the optical waveguide is a few nanoseconds for the p–i–n-diode considered here. This restriction on the modulation rate can be overcome, because the frequency transfer function (the dependence of the optical signal amplitude on the modulating

voltage amplitude) of a modulator based in a ring resonator has the form of a step (see inset in Fig. 13c). For large amplitudes of the modulating signal, the switching time of the optical signal is considerably smaller than the time in which the p–i–n-diode comes to the stationary regime. The increase in the amplitude of the modulating signal also reduces the time of removing carriers from the optical waveguide, which is inversely proportional to the reverse bias voltage. It is shown that the use of the nonstationary regime of injecting charge carriers with the modulating-signal amplitude above 3 V reduces the switching time by two orders of magnitude, down to a few ten picoseconds [108].

The modulation rate can be further increased using a reverse-biased p–n-diode in the charge-carrier separation regime in the optical waveguide [115]. In this configuration, the modulation efficiency decreases; however, the speed — restricted by the barrier capacity and by the velocity of charge carriers — considerably increases.

The use of hybrid structures based on electro-optic polymer [124] or lithium niobate [125] surface films removes restrictions related to the time of removing carriers from the waveguide and further increases the speed. However, the manufacturing technologies of hybrid structures are not very compatible with standard technological processes in microelectronics; in addition, because of the relatively low stability, these structures cannot be subjected to some technological operations, for example, they have temperature restrictions at subsequent technological stages.

The high Q-factor of ring resonators causes some problems in using them in modulators. The high intensity of optical radiation in the ring near the resonance results in nonlinear optical effects such as the Kerr effect, stimulated Raman scattering, and two-photon absorption, and also in secondary effects such as the generation of free carriers due to two-photon absorption and the thermo-optic effect caused by the absorption of optical radiation. The nonlinear characteristics of ring resonators are widely used for various applications [112]; however, their influence in modulators can produce instabilities in the operation [124]. Therefore, the power of a modulated optical signal in modulators based on ring resonators is considerably restricted and does not exceed, as a rule, 1 mW.

The high spectral selectivity makes ring resonators very sensitive to the accuracy of technological manufacturing processes. Very small deviations from a specified configuration can cause considerable distortions of the resonance peak. The situation is aggravated by the miniature size of the waveguide ring. To provide good reproducibility of characteristics of ring resonators, various methods of active thermoelectric tuning have been proposed, as has passive tuning by modifying the waveguide structure or introducing mechanical stresses [112].

Another problem facing the developers of modulators based on ring resonators is a noticeable sensitivity to variations in the external conditions, first and foremost temperature [125]:

$$\frac{\mathrm{d}\lambda}{\mathrm{d}T} = \left(n_{\mathrm{eff}}\,\alpha_{\mathrm{sub}} + \frac{\partial n_{\mathrm{eff}}}{\partial T}\right)\frac{\lambda_0}{n_{\mathrm{g}}}\,, \tag{16}$$

where λ_0 is the resonance wavelength, n_{eff} is the effective refractive index, and α_{sub} is the temperature expansion coefficient of a substrate. The temperature sensitivity is estimated at ~ 0.11 nm K^{-1} [125].

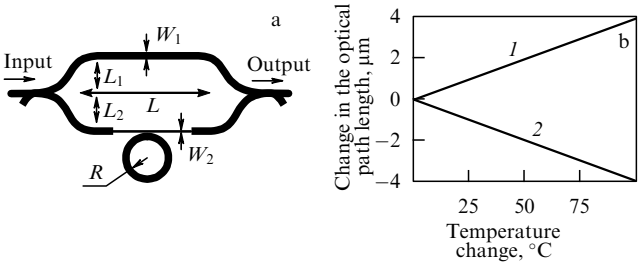

Figure 14. (a) Schematic of a modulator based on a ring microresonator inserted into a Mach–Zehnder interferometer. W_1 and W_2 are the widths of waveguides in arms *1* and *2*, respectively. (b) Temperature dependence of the optical path length. (*1*) Effective optical path of the ring, (*2*) effective optical length of the Mach–Zender interferometer arms.

In the literature, two main avenues for solving the problem of reducing the temperature influence are considered. The first is the passive compensation of the temperature drift by creating so-called athermal devices insensitive to temperature variations.

An additional cover with a negative expansion coefficient compensates the influence of the positive expansion of silicon [126]. As a material with a negative temperature expansion coefficient, titanium dioxide TiO_2 is often used [127]. This technology provided the compensation of the temperature dependence of the resonance shift equal to 5 pm K^{-1} in the temperature region of 50 K [128].

Another example of the passive compensation of the temperature drift is the inclusion of a ring resonator in the arm of a compensation Mach–Zehnder interferometer [129]. The width of waveguides in different arms of the Mach–Zehnder interferometer is selected so that temperature variations in the difference among optical paths in the interferometer arms compensate temperature changes in the optical length of the ring resonator (Fig. 14).

The second avenue is the use of active compensation based on feedback temperature-control systems. The temperature of a ring resonator can be controlled by varying a direct current flowing through a system of modulator electrodes. However, it is more convenient to use independent local heaters integrated into a chip and located near or even inside the waveguide ring of the resonator [130]. In principle, the entire control system can be completely integrated on a chip together with a modulator, including a photodetector and electronics controlling the heater [131]. A disadvantage of this approach is the additional energy consumption, which is estimated to be from 25 to 55 fJ bit^{-1} for a transfer rate of 10 Gbit s^{-1} [132–134].

Another popular method for creating modulators uses an optical filter based on a reflection Bragg grating combined with a waveguide [135, 136]. An applied electric field changes the refractive index, which results in a shift of the reflected Bragg wavelength λ_{B} (Fig. 2f):

$$\lambda_{\mathrm{B}}(E_{\mathrm{ext}}) = 2n(E_{\mathrm{ext}})\Lambda\,. \tag{17}$$

Here, Λ is the lattice period and E_{ext} is the control electric field.

A strong dispersion near the central Bragg reflection wavelength can be used not only for amplitude but also for phase modulation or to control the delay of optical pulses [137]. As in the case of resonance modulators based on the shift of the resonance wavelength, the width of the Bragg

reflection band imposes considerable restrictions on the modulation frequency band [138].

4.5 Controllable directional coupler

Along with the types of modulators considered in Section 4.1–4.4, many other setups for using electrically controlled waveguides have been developed [139]. Such devices appeared mainly in the first years of the development of technology of integrated optical modulators, but some of them still exist. One of them is a controllable directional coupler.

A typical directional coupler is shown in Fig. 2g. Two waveguides separated by a distance sufficient for their interaction provide the division of the optical power between the arms in a proportion specified by the voltage. A separation electrode [140] is used to compensate errors that appear during their manufacture.

A directional coupler is not so fast a modulator as an MZM, but it is used as a good compact high-speed switch. Couplers in the form of a tree-like setup were mainly used to demonstrate multichannel integrated optical switches [141].

5. Construction of electrodes in broadband integrated optical modulators

5.1 Traveling-wave electrodes

A constructive feature of integrated optical modulators is that the interelectrode gap is about 10 μm, whereas the interaction length should be made as large as possible to decrease the control voltage. In the case of electro-optic modulators on lithium niobate substrates, the length of the electrodes can be several centimeters, which exceeds the wavelength of the modulating signal with a modulation frequency of 10 GHz and above. For this reason, to provide effective modulation, a traveling wave technique is used, where a voltage wave propagates along electrodes with the same velocity as the propagation velocity of an optical wave in the waveguide and in the same direction. In the absence of losses in microwave electrodes, the operation band of such a modulator would not be restricted [142]. Any difference between the velocities of two waves produces a phase incursion, which increases with increasing frequency or interaction length, and finally restricts the frequency band of the modulator [19]:

$$B = \frac{1.4c}{\pi|n_{\text{eff}} - n_{\mu}|L}\,, \tag{18}$$

where B is the modulation band of the electric signal, n_{eff} and n_{μ} are optical and microwave effective refractive indices, and c is the speed of light in a vacuum (Fig. 15). The quantity B, as a rule, is expressed in terms of the parameter $\xi = \pi L|n_{\text{eff}} - n_{\mu}|/c$ determining the mismatch of the phase velocity of the modulating electric field and the group velocity of the optical wave.

In the ideal case, the characteristic impedance of electrodes should coincide with the usual system impedance of 50 Ω to avoid large signal reflections; however, exact coincidence is usually difficult to obtain.

Figure 16 shows the most popular types of electrodes used in electro-optic modulators. The first type is so-called lumped electrodes in the form of a capacitor (Fig. 16a). The other two types are electrodes providing the operation of the modulator in the microwave wavelength range. Distributed microwave electrodes in the form of a coplanar microstrip line (Fig. 16b)

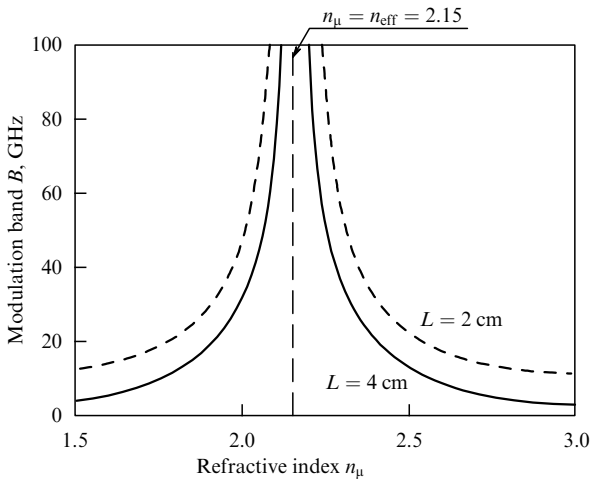

Figure 15. Dependences of the frequency band B on the velocity mismatch for different interaction lengths.

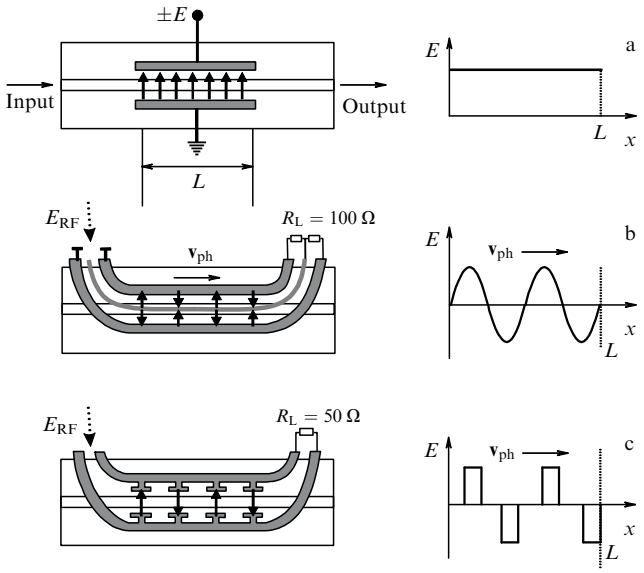

Figure 16. Types of electrodes (left) and the electric field distribution along the electrodes (right). (a) Lmped capacitive electrodes, L is the length of the electrodes, (b) traveling-wave microwave electrodes base on a coplanar line (a coplanar line has a central strip), $\mathbf{v}_{\text{ph}}$ is the phase velocity of a traveling electric wave, two load resistances $R_{\text{L}} = 100\ \Omega$, (c) segmented electrodes with capacitive coupling. This case is a combination of (a) and (b). E_{RF} is the input microwave electric signal, one load resistance $R_{\text{L}} = 50\ \Omega$.

are typical for electro-optic lithium niobate modulators. A discrete configuration in the form of the structure of segmented lumped electrodes with capacity coupling (Fig. 16c) is used in semiconductor modulators [143].

5.2 Factors affecting the optimal configuration of microwave electrodes

The fundamental principle underlying the designing of broadband modulators is the search for some compromise between the bandwidth and control voltage. Consider the main factors that should be taken into account in the construction of microwave electrodes by using the example of a lithium niobate electro-optic modulator.

Lithium niobate is convenient for use in integrated optical circuits. However, lithium niobate is a ferroelectric, and its permittivity in the microwave region ($\varepsilon_x^{\mu} = 28, \varepsilon_y^{\mu} = \varepsilon_z^{\mu} = 43$) is considerably higher than in the optical region ($\varepsilon_x^0 = n_e^2 \approx 4.6$)

[21, 144]. This complicates the creation of a broadband microwave modulator. In most integrated lithium niobate optical devices, an optical waveguide and an optical wave propagating in it lie inside a substrate. This means that the effective refractive index of the optical wave is close to the refractive index of lithium niobate. The only way to match velocities in this case is to change the configuration of traveling-wave electrodes so as to reduce the part of the microwave field propagating through the lithium niobate and create such a configuration where a considerable part of the field would propagate through materials with a lower refractive index at microwave frequencies (air, silicon dioxide, etc.).

One of the simplest configurations of microwave electrodes is a coplanar waveguide formed on a plane surface (Fig. 17). Velocity matching in this configuration can be achieved by increasing a buffer layer consisting of a material (SiO_2) with a low refractive index, which increases the half-wave voltage for the same length of electrodes. The velocity matching can be also improved by increasing the thickness of the electrodes. In this case, most of the electric field propagates in the air gap between electrodes, reducing the effective refractive index. However, the manufacture of thick electrodes with a narrow air gap is a complicated technological issue.

The second limiting factor is the energy losses of a microwave in the electrode material and in dielectrics of the coplanar line (see Fig. 17). Due to the skin effect at high frequencies, the current mainly flows over the external surfaces of the electrodes, while the dominance of the inductive component of a resistance per unit length over the resistive component causes the flow of current mainly over the surfaces of adjacent electrodes facing each other. The losses can be reduced by using thick electrodes and materials with a high conductivity. Silver, having a high conductivity, possesses some advantages over gold (62.5×10^6 S m^{-1} vs 45.5×10^6 S m^{-1}) [145].

The third limiting factor, as already mentioned, is the mismatch between the wave impedance of microwave electrodes of the modulator and the wave impedance of 50 Ω of the input tract, which results in an increase in the backward reflection coefficient and the degradation of characteristics of the modulator in the low-frequency region.

The fourth limiting factor is inefficient modulation because of the small product of the integral of the field penetrating onto the optical waveguide by the operating electro-optic coefficient. The modulation efficiency related to this factor is characterized by the quantity $V_\pi L$, where V_π is the half-wave voltage of the modulator and L is the interaction length of microwave electrodes. The smaller $V_\pi L$ is for the modulator, the lower the voltage and therefore power required at the modulator microwave input for controlling optical radiation for the same modulator length. The increase in the interaction length not only results in an increase in the physical size of the modulator, but also deteriorates the frequency band of the modulator, because the velocity mismatch and losses in microwave electrodes increase with increasing interaction length. The frequency dependence of the electro-optic response of the modulator is described by the expression [19]

$$H(f) = \sqrt{\frac{1-2\exp\left(-\alpha(f)L\right)\cos\left(2\xi f\right)+\exp\left(-2\alpha(f)L\right)}{\left(\alpha(f)L\right)^2+\left(2\xi f\right)^2}}, \tag{19}$$

where $\alpha(f) = \alpha_e\sqrt{f}$ is the frequency-dependent decay of an electric signal in electrodes caused by the skin effect and α_e [Np (m Hz$^{1/2}$)$^{-1}$] is the decay coefficient.

Note that constrictive decisions taking into account any of the above factors are, as a rule, in conflict with decisions based on the consideration of other factors. Thus, for the simplest configuration of a coplanar line with a buffer layer (see Fig. 17), exact velocity matching can be achieved with the geometrical parameters $W = 8$ μm, $G = 15$ μm, $T_b = 0.9$ μm, and $T_e = 20$ μm. In this case, the product $V_\pi L$ becomes 13 V cm and the wave impedance is 35 Ω. To achieve the matching of the wave impedance with the source of 50 Ω, the value of T_b should exceed 2 μm. In this case, $V_\pi L$ increases to 20 V cm.

In the literature, numerous configurations of lithium niobate traveling-wave electro-optic modulators have been considered in which different variants for solving these contradictions were proposed. These solutions involve complicating the form of the electrodes and the use of etching and special materials for a dielectric buffer layer (Fig. 18) [146].

6. Basic characteristics of modern modulators

In this section, we define some general characteristics of modulators, lay out criteria to estimate them and present the state-of-the-art level.

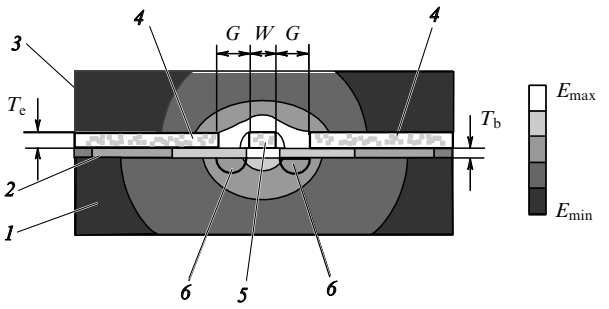

Figure 17. Electric field distribution in the cross section of traveling-wave microwave electrodes made in the form of a coplanar line. A Mach–Zehnder amplitude modulator on an X-cut substrate. (*1*) $LiNbO_3$ substrate, (*2*) SiO_2 buffer layer, (*3*) air, (*4*) electrodes, (*5*) central 'grounded' electrode, (*6*) optical waveguides, G is the distance between electrodes, W is the width of the 'grounded' electrode, T_e is the buffer layer thickness, T_b is the thickness of electrodes.

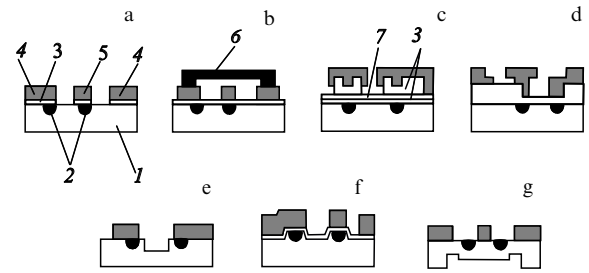

Figure 18. Examples of configurations of microwave electrodes based on microstrip lines with a complicated profile. (a) Modulator with an etched buffer layer, (*1*) substrate, $LiNbO_3$ Z-cut, (*2*) optical waveguides, (*3*) SiO_2 buffer layer, Au electrons, (*4*, *5*) microwave electrodes in the form of a coplanar line. (b) Structure with a screening electrode *6*. (c) Modulator with a buried buffer layer, an additional Si layer, (d) modulator with a mushroom 'hot' electrode and a step buffer layer, (e) modulator with a groove between electrodes, a buffer layer is absent, (f) modulator with ridge optical waveguides, (g) modulator with a two-step back, the X-cut.

6.1 Switching voltage

The switching voltage is one that should be applied at the modulator input to switch from the maximum of optical transmission to its minimum.

When the frequency transfer function of a modulator has a periodic shape, the half-period of the transfer function can be uniquely defined. The switching voltage for amplitude modulators based on interferometers (for example, MZMs) is called a half-wave voltage V_π, because the phase shift by π between the interferometer arms reduces the output intensity from its maximum to minimum. For an MZM with a linear electro-optic effect, the switching voltage V_π is

$$V_\pi = \frac{\lambda_0}{n^3 r L} \frac{\int\int \mathrm{d}x\,\mathrm{d}y\, I(x,y)}{\int\int \mathrm{d}x\,\mathrm{d}y\, \tilde{E}(x,y) I(x,y)} . \tag{20}$$

Here, λ_0 is the wavelength of light in a vacuum, L is the length of electrodes in a modulator, $I(x,y)$ is the intensity distribution of a waveguide mode, and $\tilde{E}(x,y) = E(x,y)/V$ is the electric field divided by the voltage applied to electrodes. The typical half-wave voltage of modern integrated optical modulators is ~ 5 V.

Reducing the half-wave voltage is one of the key problems in the further development of the technology of broadband modulators. Because the main technological platforms and materials for the development of integrated optical modulators are already determined, the main trend is the optimization of the configuration of electrodes and the optical scheme, the compression of the transverse size of waveguide modes, and the increase in the modulation efficiency by increasing the intensity of the optical and modulating microwave field (denominator in expression (12)). The use of optical waveguides with a high contrast of the refractive index has provided half-wave voltages below 1.5 V for reasonable interaction lengths [147].

If the frequency transfer function is not periodic, the switching voltage is defined as the voltage required to switch from a high transfer level to some decay level. For example, 'V_{10}' means that this voltage corresponds to switching to the level of -10 dB. In analog problems, the main parameter is the maximum slope ($\mathrm{d}T/\mathrm{d}V$) of the frequency transfer function, which is expressed as 'the equivalent half-wave voltage V_π' ($V_{\pi\mathrm{e}}$):

$$V_{\pi\mathrm{e}} = \frac{\pi}{2} \left| \frac{\mathrm{d}T}{\mathrm{d}V} \right|^{-1}_{\max} . \tag{21}$$

This characteristic allows one to compare modulators of any type. Note that the switching voltage increases if the modulator is not matched in the impedance. This problem is typical for modulators based on materials with high dielectric constants in which the wave impedance of electrodes is usually below 50 Ω.

In digital systems, the characteristic related to the switching voltage is called the 'control voltage'. This is the doubled voltage amplitude of a pseudorandom sequence of bits required to achieve the required extinction in the eye diagram. The control voltage can be both greater and smaller than the switching voltage.

The switching voltage is an important characteristic, because it determines the power (amplitude) of an electric signal required to control the modulator. For analog applications, the switching voltage is one of the main parameters determining the noise coefficient.

6.2 Frequency responses of modulators

The frequency responses of a modulator are measured using a network analyzer and a calibrated photodetector. The known transfer function of a detector is removed from the total response to obtain characteristics for the modulator only. Note that the output electric power of the photodetector is proportional to the square of the direct component of the optical power and inversely proportional to the square of the switching voltage. To perform correct measurements, it is necessary to avoid the transfer of the photodetector to the saturation regime. The operating point of the modulator should be at the quadrature point (in the linear part of the frequency transfer function), while the modulation amplitude should be smaller than $0.1\,V_\pi$ to minimize the influence of nonlinear distortions. Figure 19 presents an example of the electric frequency transfer function of an integrated optical MZM developed by the Ioffe Institute together with the National Research University of Information Technologies, Mechanics and Optics [148]. Note that the frequency responses of the modulator are affected by impedance matching. The electric input port of the modulator must not reflect an applied electric signal. This can be achieved either by manufacturing a modulator with the internal impedance equal to the system impedance (usually 50 Ω) or making matching transformers. The frequency dependence of reflections is measured with a network analyzer simultaneously with the measurement of the frequency transfer functions.

The electric frequency transmission band is defined quite simply as the frequency at which the output signal of a photodetector drops 3 dB below its low-frequency value. Nevertheless, different manufacturers of modulators define this characteristic differently. The reason is the nonmonotonic behavior of the frequency transfer function in the low-frequency region due to various reasons:

— The resistive and capacitance division of voltage between different layers of the modulator structure. Usually, this affects frequencies from fractions of a hertz to ~ 1 MHz [149];

— The excitation of acoustic waves. The problem is manifested up to frequencies of ~ 1 GHz. Acoustic resonances in a substrate are very sharp, are often narrower than 100 kHz, and have amplitudes above 1 dB [150].

Note that the basic properties of crystals change with increasing frequency from the state of 'free' crystals to the state of 'clamped' crystals. For lithium niobate, this occurs at frequencies of < 100 MHz [151] and causes a decrease in the signal of almost 1 dB. The frequency band of modulators is often measured with respect to the relatively low-frequency point at a higher frequency than these parasitic effects (~ 1 GHz).

For traveling-wave electrodes, there is a fundamental restriction on the frequency band determined by ohmic losses in electrodes increasing with the increase in frequency caused by the skin effect. When the electric and optical velocities coincide, the frequency-dependent switching voltage at the input impedance of the modulator has the form

$$V_\mathrm{s}(f) = V_{\mathrm{s,DC}} \sqrt{\frac{Z_\mathrm{i}}{Z_0}} \frac{\delta_\mathrm{p}(f) L/2}{1 - \exp\{-\delta_\mathrm{p}(f) L/2\}} . \tag{22}$$

Here, Z_i is the input impedance of the system, Z_0 is the impedance of the modulator transfer line, $\delta_\mathrm{p}(f)$ is frequency-dependent electric power losses per unit length of electrodes, and DC in $V_{\mathrm{s,DC}}$ is the DC switching voltage applied directly to the electrodes. One can see from (22) that the frequency band can be broadened by decreasing the length; however, as

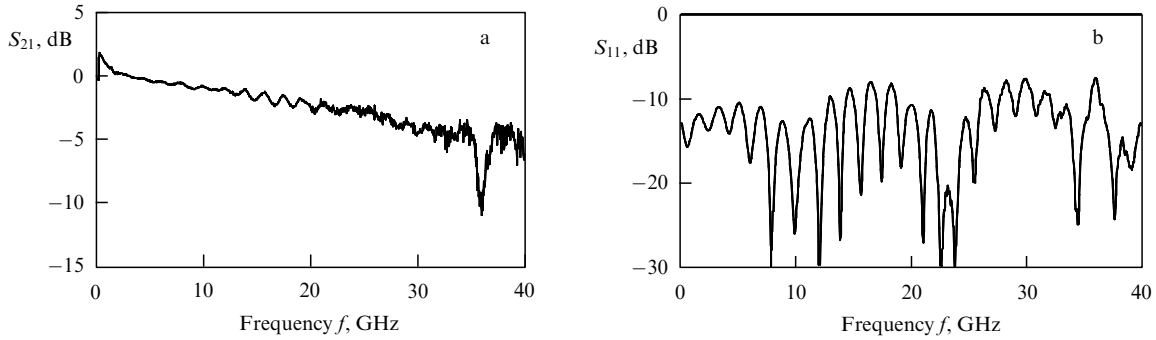

Figure 19. Dependences of parameters S_{21} and S_{11} of an amplitude modulator based on a Mach–Zehnder interferometer on the input-signal frequency.

mentioned above, a compromise exists between the modulation frequency band and the control voltage. For modulators based on waveguides on lithium niobate substrates, the maximum width of the frequency band at the 3 dB level reaches ≈ 40 GHz for typical control voltages of ≈ 5 V. For this reason, in studies where modulation at frequencies of 100 GHz and above was demonstrated, the control voltage, as a rule, exceeded 10 V and the decay of the frequency response was more than 5 dB. The use of thin-film lithium niobate allows the frequency to be increased due to an increase in the modulation efficiency and a considerable decrease in the modulator length [152]. Thin-film lithium niobate offers additional advantages for preventing parasitic microwave resonances due to excitation of substrate modes [153]: a lithium niobate substrate itself serves as a dielectric microwave waveguide. In the region of the imperfect coupling of a microwave tract with a coplanar line of electrodes, a partial leaking of a modulating microwave signal occurs to substrate modes, which interfere with a mode propagating in traveling-wave electrodes [154]. This results in pulsations at the frequency response and resonances in the high-frequency region. A resonance at the frequency of ≈ 36 GHz corresponding to excitation of the modes of a 1-mm-thick lithium niobate substrate can be observed in the frequency transfer function in Fig. 19. Because of this, to broaden the frequency band, two-step back-slot (Fig. 18g) are commonly used. To shift resonances by frequencies above 100 GHz, the substrate thickness in the region of the electrodes must be reduced to 100 μm or more [155, 156].

The length of semiconductor modulators is considerably smaller than that of lithium niobate modulators, and therefore ohmic losses do not restrict their frequency band. The bandwidth restriction is determined by the large capacity of the semiconductor structure, which not only prevents broadening of the frequency band but also complicates the matching of the impedance with the input microwave tract of 50 Ω. The frequency responses of III–V semiconductor modulators are comparable to these of lithium niobate modulators. The characteristics of silicon modulators are greatly inferior, which is related to the inertia of the plasma-dispersion effect.

6.3 Other characteristics: optical losses, optical spectral band, modulation contrast, chirp, and linearity

The coefficient of optical losses is the output optical power divided by the input optical power when a modulator is shifted to the maximum transfer of the optical power. Optical losses are important for any application: they directly enter the transfer coefficient of a system. Note that the total optical losses contain two components: the internal losses of optical waveguides and the optical fiber coupling losses. The typical internal losses for lithium niobate waveguides are of the order of 0.2 dB cm^{-1}.

Many studies on matching a guided mode with a mode of an optical telecommunication fiber [157–159] resulted in the lowering of total losses (fiber–fiber) to 2–3 dB. The internal losses in semiconductor waveguides are considerably higher; however, they are compensated due to the smaller length of the modulator. Such semiconductor waveguides have a considerably inferior matching between the guided mode and the mode of the optical fiber. All this leads to higher total optical losses of semiconductor modulators (4–5 dB) than those in lithium niobate modulators.

The maximum optical power at which a modulator can operate is related to optical losses. While digital problems require powers from 1 to 10 mW, analog problems usually require higher powers, up to 2.5 W. Lithium niobate modulators have a very high damage threshold, and the main restricting factors are the optical nonlinearity and photorefractive effect. The typical maximum optical power of lithium niobate modulators is 200 mW. Semiconductor modulators operating near the resonance absorption region do not possess such a high damage threshold and therefore they are rarely used in problems where the optical power exceeds 10 mW. Note, however, that the III–V semiconductor modulators can be integrated with an optical amplifier capable of increasing the output optical power of this device up to a few ten milliwatts [160].

The optical spectral band of a modulator is the wavelength range in which the modulator operates. To determine the optical spectral band, all the key characteristics (electric band, switching voltage, extinction coefficient, chirp, and linearity) should be measured at different wavelengths to find out their unacceptable values. These characteristics are the most important for systems operating simultaneously at several wavelengths, although such applications are used quite rarely. The requirement is usually reduced to the necessity of working at an arbitrary wavelength from the specified spectral range.

Note that the optical band of lithium niobate electro-optic modulators is wider than that of semiconductor modulators. Taking into account a weak enough dispersion of the characteristics of lithium niobate in the visual and near-IR spectral ranges, the optical band of lithium niobate modulators is determined by the spectrum region of the single-mode

propagation regime in optical waveguides. Even in thin-film lithium niobate waveguides with a considerable waveguide dispersion due to the great difference between refractive indices, the single-mode propagation region can cover the entire telecommunication wavelength range from 1500 to 1600 nm. Semiconductor modulators use dispersion effects to modulate optical radiation, and therefore their optical band is much narrower. The control voltage for III–V semiconductor modulators can change almost twice in the C-region of telecommunication wavelengths (1530–1560 nm) [161].

The optical contrast of the modulation (extinction ratio) is the ratio of the optical power in the transmission maximum to the optical power in the transmission minimum of the frequency transfer function of the modulator. This ratio is infinite for an ideal symmetric MZM. In practice, this is not the case at all. Figure 20 shows the statistical dependence of the output optical power on the applied voltage for a lithium niobate MZM. A high optical contrast is not required for all practical applications. A low optical contrast results in an energy loss in a digital communication and a slight deterioration of the transfer coefficient in analog systems in microwave photonics. Therefore, requirements for the optical contrast in these applications are not high, no more than 20 dB [162]. New applications related to quantum telecommunications [163] and systems for processing signals from distributed fiber-optic detectors [164] raise many more strict requirements for the optical contrast, more than 40 dB, and sometimes more than 60 dB. Numerous methods have been proposed both for the active balance [165] of waveguide interferometers using a feedback optoelectronic system and the passive balance [166] for obtaining an optical modulation contrast above 50 dB.

In digital applications, the optical contrast partially determines the parameters of eye diagrams. Eye diagrams are not the best method for estimating the characteristics of a modulator, because they mix together several characteristics. In addition, it is difficult to separate the influence of the modulator from the influence of other components of the system. However, this method is quite often used because of its simplicity and direct relation to digital applications. It should be taken into account that an eye diagram contains, along with the contribution of the modulation contrast, contributions from electric reflections, the slope of the frequency response, and a chirp caused by the dispersion of an optical fiber. Frequency jitter is commonly related to electric reflections, and although the modulator itself does not cause the jitter, it can facilitate the appearance of jitter if it has electric reflection. The rise time is determined by the frequency response of the modulator.

The parameter η characterizing the chirp — the ratio of the change in the frequency of an optical carrier to the rate of the intensity change upon amplitude modulation [167, 168] — is described by the expression

$$\eta = \frac{\mathrm{d}\phi}{\mathrm{d}t}\,\frac{2I(t)}{I'(t)} = \frac{4\pi\Delta f I(t)}{I'(t)}\,. \tag{23}$$

Here, $I(t)$ is the optical intensity, $I'(t)$ is the time derivative of the intensity, $\mathrm{d}\phi/\mathrm{d}t$ is the phase-change rate, and $\Delta f(t)$ is the change in the carrier frequency. It can be seen from (23) that the chirp appears only on the increasing or decreasing edges of a pulse when derivatives are nonzero. For an ideal MZM based on the linear electro-optic effect, the parameter η depends on the bias. At the quadrature point (half of the transmission maximum), it takes a simple form

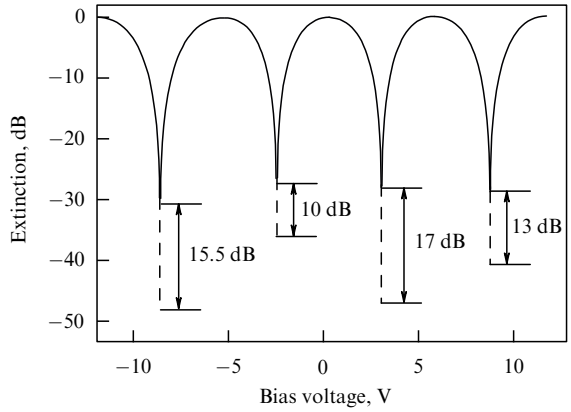

Figure 20. Statistical dependence of the output optical power (expressed in decibels with respect to the optical power at the transmission maximum) on the applied voltage for a lithium niobate MZM. Solid curve: before photorefractive balancing of the interferometer, dashed line: after photorefractive fit of the interferometer.

$$\eta = \frac{\Delta V_2 + \Delta V_1}{\Delta V_2 - \Delta V_1}\,. \tag{24}$$

The importance of this result is that the phase shift in the modulator arm linearly depends on the applied voltage function. A doubly controlled MZM can be used to correct the chirp [169]. The zero chirp corresponds to the ideal two-cycle modulation $V_1(t) = -V_2(t)$, then the parameter $\eta = 0$. A symmetric modulator with $V_1(t) \neq -V_2(t)$ gives either a positive or negative chirp, depending on control voltages; $|\eta| < 1$, when fields are in phase opposition, and $|\eta| > 1$, when field are in phase. The special case for a modulator with one control voltage is $\eta = \pm 1$.

The parameter η is also important for III–V semiconductor MZMs [170]. However, controlling chirp in semiconductor modulators is more complicated because of the nonlinear dependence of the phase shift on the voltage.

Note that the description of chirp with one numerical parameter η is a strong simplification. The frequency change in the modulation process is a complicated time-dependent function. Ideally, it is necessary to measure a change in the carrier frequency upon modulation (time-resolved chirp); however, this is difficult to perform due to high modulation frequencies and restrictions imposed on simultaneously achieving a high resolution in time and frequency.

The linearity of the frequency transfer function of a modulator is especially important for analog measurements in microwave photonic systems and processing signals from fiber-optic sensors. As a rule, the coefficients of second- and third-order intermodulation distortions reduced to the input are used [4–6]. They determine the level of the electric power at the modulator input at which the power of the corresponding intermodulation component detected at the modulator output becomes equal to the power of the fundamental component (Fig. 21).

Second-order intermodulation distortions in an electro-optic MZM at the quadrature working point are zero, which is especially important for broadband applications. Such a modulator can be used in super octave systems in which the transition bandwidth exceeds an octave (i.e., the upper cut-off

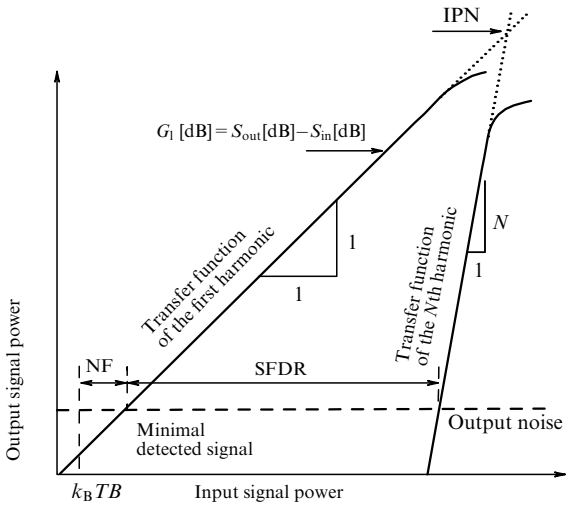

Figure 21. Determination of the coefficient of nonlinear distortions and the SFDR (Spurious Free Dynamic Range). k_BTB is the thermal noise power in the frequency band B, NF (Noise Figure) is the noise coefficient. SFDR is the spectral range free of nonlinear distortions, G_1 is the linear transfer coefficient, S_{in} is the input signal, S_{out} is the output signal, N is the number of an intermodulation component, IPN (Intersection Point of N-order) is the point of intersection of the fundamental component with the intermodulation component of N-order.

frequency is more than twice the lower cut-off frequency). The linearity of semiconductor modulators with a complicated nonlinear response is considerably worse.

Nonlinear distortions determine the upper boundary of the dynamic range free from nonlinear distortions. The typical value of the coefficient of intermodulation distortions reduced to the input for an MZM with the half-wave voltage $V_\pi = 5$ V is IIP3 ≈ 100 mW (20 dBm), this parameter decreasing with a decrease in the half-wave voltage. However, the dynamic range does not narrow in this case, because the decrease in the half-wave voltage causes an increase in the transfer coefficient. The lower boundary of the dynamic range is limited by the noise level, which is, as a rule, determined by the laser noise. Noises introduced by a lithium niobate electro-optic modulator are related to the thermal noise of the load resistance of traveling-wave electrodes and are negligible. The typical spurious-free dynamic range (SFDR) for lithium niobate MZM systems is about 100 dB $Hz^{-2/3}$ with the use of a laser diode with the relative intensity noise (RIN) RIN ≈ -150 dB Hz^{-1}. The noise coefficient of semiconductor modulators is somewhat higher and can reach a few decibels, which, together with the lower coefficient of intermodulation distortions, will considerably narrow the dynamic range of optical systems using such modulators.

The frequency transfer functions of integrated optical modulators are linearized by many methods [171, 172]. The linearization is based on the suppression of intermodulation components due to the interference of several modulated signals. Systems of modulators for linearization are based, as a rule, on complex composite interferometers. The use of linearized modulators provides an expansion of the dynamic range to the level of 125 dB $Hz^{-2/3}$ or more.

7. Conclusions

Progress achieved in the last 30 years in the field of integrated broadband optical modulators has brought optical information systems to a fundamentally new level. The achieved modulation frequency bands above 100 GHz and control voltages below 1 V, as well as new designs of modulators providing special modulation formats of optical signals, have increased the transmission capacity of optical communication lines close to the theoretical limit for optical fibers.

Semiconductor modulators are the most convenient ones for digital applications in which a low control voltage is especially important, while the response nonlinearity typical of them, the quite high noise level, and restrictions on the optical power are not such critical factors and do not noticeably affect the transmission capability.

III–V semiconductor modulators are the most popular devices used in modern fiber-optic communication lines. Their most important distinguishing feature is the possibility of integrating them into complex photonic setups [173] due to the miniature size and well-developed technologies of laser diodes, semiconductor amplifiers, and high-frequency photodetectors using the same material platform.

Commercially available silicon modulators to date have not been able to provide the high modulation frequencies required in fiber-optic communication channels. Modulation frequencies attainable at present are ~ 10 GHz, but this area is very rapidly developing. The most interesting thing here is modulators based on ring resonators providing a small size, a high efficiency, and a very high modulation rate in sight, while the compatibility of technology of silicon modulators with the metal–oxide-semiconductor complementary structure technology of digital electronic circuits makes them the main candidates for optical coupling between chips and inside chips in processors [174–176].

Lithium niobate is the oldest material platform for manufacturing integrated optical modulators. Although the first lithium niobate integrated optical modulators appeared almost 50 years ago, these devices are still finding their niche for practical applications, first of all analog applications in systems of microwave photonic and processing signals from fiber-optic sensors, where the high linearity, the low level of introduced noise, and the possibility of operating with an optical power of a few hundred milliwats determine their leadership with respect to semiconductor modulators.

Another field of applications of lithium niobate modulators is systems of quantum information photonics [177] in which, aside from the low noise coefficient important in the case of single-photon signals, the unique properties of lithium niobate open up the possibility of creating other key elements, such as sources of entangled states, quantum memory cells, and systems of linear calculations.

The further development of lithium niobate integrated optical modulators is related to the recent thin-film $LiNbO_3$ technology [178], which not only considerably improves the key characteristics (broadening the frequency band above 100 GHz and reducing the control voltage below 1.5 V), but also opens up possibilities for hybrid integration with semiconductor optoelectronics [179].

References

1. Yariv A, Yeh P *Photonics*: *Optical Electronics in Modern Communications* (New York: Oxford Univ. Press, 2007)
2. Agrawal G P *Fiber-Optic Communication Systems* (New York: Willey, 2010)
3. Mahapartha A, Murphy E J, in *Optical Fiber Telecommunications IV. A. Components* (Eds I P Kaminow, T Li) (San Diego, CA: Academic Press, 2002) p. 258

4. Chen A, Murphy E *Broadband Optical Modulators*: *Science, Technology, and Applications* (Boca Raton, FL: CRC Press, 2012)
5. Chang W S C (Ed.) *RF Photonic Technology in Optical Fiber Links* (Cambridge: Cambridge Univ. Press, 2002)
6. Urick V J (Jr.), McKinney J D, Williams K J *Fundamentals of Microwave Photonics* (Hoboken, NJ: Wiley, 2015); Translated into Russian: *Osnovy Mikrovolnovoi Fotoniki* (Moscow: Tekhnosfera, 2016)
7. Udd E, Spillman W B (Jr.) (Eds) *Fiber Optic Sensors*: *An Introduction for Engineers and Scientists* (Hoboken, NJ: John Wiley and Sons, 2011) p. 87
8. Rediker R H, Lind T A, Burke B E *J. Lightwave Technol.* **6** 916 (1988)
9. Liu Z et al. *J. Lightwave Technol.* **38** 1844 (2020)
10. Huiszoon R J W et al. *J. Lightwave Technol.* **23** 1116 (2020)
11. Lau K Y, in *Dynamics of Quantum Well Lasers* (Eds K Y Lau, S Zory (Jr.)) (San Diego, CA: Academic Press, 1993) p. 217
12. Okiyama T et al. *J. Lightwave Technol.* **6** 1686 (1998)
13. Kikuchi K *J. Lightwave Technol.* **34**157 (2016)
14. Sivukhin D V *Obshchii Kurs Fiziki* (General Physics Course) (Moscow: Fizmatlit, 2002)
15. Pankove J I *Optical Processes in Semiconductors* (New York: Dover Publ., 1971)
16. Miller D A B et al. *Phys. Rev. Lett.* **53** 2173 (1984)
17. Yariv A *Introduction to Optical Electronics* (New York: Holt, Rinehart and Winston, 1976)
18. Li G, Yu P *J. Lightwave Technol.* **21** 2010 (2003)
19. Petrov V M, Shamrai A V *Interferentsiya i Difraktsiya dlya Informatsionnoi Fotoniki* (Interference and Diffraction for Information Photonics) (St. Petersburg: Lan', 2019)
20. Weis R, Gaylord T *Appl. Phys. A* **37** 191 (1985)
21. Toney J E *Lithium Niobate Photonics* (Norwood: Artech House, 2015)
22. Bazzan M, Sada C *Appl. Phys. Rev.* **2** 040603 (2015)
23. Karavaev P M et al. *Tech. Phys. Lett.* **42** 513 (2016); *Pis'ma Zh. Tekh. Fiz.* **42** (10) 33 (2016)
24. Il'ichev I V et al. *Quantum Electron.* **39** 98 (2009); *Kvantovaya Elektron.* **39** 98 (2009)
25. Betts G F, O'Donnell F J, Ray K G *IEEE Photon. Technol. Lett.* **6** 211 (1994)
26. Fujivara T, Sato S, Mori H *Appl. Phys. Lett.* **54** 975 (1989)
27. Betts G E, Ray K G, Johnson L M, Integrated Photonics Research, Technical Digest (Washington, DC: OSA, 1990) p. 37
28. Varlamov A V et al. *Tech. Phys. Lett.* **43** 994 (2017); *Pis'ma Zh. Tekh. Fiz.* **43** 87 (2017)
29. Petrov A N et al. *Tech. Phys.* **60** 761 (2015); *Zh. Tekh. Fiz.* **85** 131 (2015)
30. Lee M et al. *Science* **298** 1401 (2002)
31. Kim T D et al. *J. Am. Chem. Soc.* **129** 488 (2007)
32. Korotky S K *J. Lightwave Technol.* **12** 2687 (1996)
33. Burns W K et al. *J. Lightwave Technol.* **17** 2551 (1999)
34. Gopalakrishnan G K et al. *J. Lightwave Technol.* **12** 1807 (1994)
35. Krahenbuhl R, Burns W K *IEEE Trans. Microwave Theory Tech.* **48** 860 (2000)
36. Cartlendge J C *IEEE Photon. Technol. Lett.* **9** 1090 (1995)
37. Macario J et al. *Opt. Express* **20** 23623 (2012)
38. Kaminov I P et al. *Appl. Phys. Lett.* **24** 622 (1974)
39. Izutsu M et al. *IEEE J. Quantum Electron.* **13** 287 (1977)
40. Rangarath T R, Wang S *Appl. Phys. Lett.* **4** 376 (1977)
41. Sasaki H *Electron. Lett.* **13** 693 (1977)
42. Makami O, Noda J, Fukuma M *Translat. IEICE Jpn.* **E-61** 144 (1978)
43. Minakata M et al. *J. Appl. Phys.* **49** 4677 (1978)
44. Alferness R C et al. *Appl. Opt.* **23** 4012 (1979)
45. Leonberger F J *Opt. Lett.* **5** 312 (1980)
46. Tench R E *J. Lightwave Technol.* **5** 492 (1987)
47. Kondo M et al. *Electron. Lett.* **23** 1167 (1987)
48. Blumenthal P R et al. *Electron. Lett.* **23** 1359 (1987)
49. Thylen L *J. Lightwave Technol.* **6** 847 (1988)
50. Sawaki I et al. *IEEE J. Selected Commun.* **6** 1267 (1988)
51. Nishimoto H et al. *IEEE Photon. Technol. Lett.* **2** 634 (1990)
52. Nozawa T et al., in *Photonic Switching II. Proc. of the Intern. Topical Meeting, 1990* (Eds K Tada, S Hinton) (Heidelberg: Springer-Verlag, 1990) p. 84
53. Fukuma M, Noda J, Iwasaki H *J. Appl. Phys.* **49** 3693 (1978)
54. Fouchet S et al. *J. Lightwave Technol.* **5** 700 (1987)
55. Nozawa T et al. *Appl. Opt.* **30** 1085 (1991)
56. Fukuma M, Noda J *Appl. Opt.* **19** 591 (1980)
57. Alferness R C et al. *Electron. Lett.* **12** 490 (1982)
58. Ramaswamy V, Alferness, Divino M *Electron. Lett.* **18** 30 (1982)
59. Komatsu K et al. *IEEE J. Lightwave Technol.* **5** 1239 (1987)
60. Kataoka T et al. *Electron. Lett.* **30** 715 (1994)
61. Hagimoto K et al., in *Conf. Optical Fiber Communications OFC 97, Dallas, TX, 1997*, p. 242
62. Kawano K et al. *Electron. Lett.* **25** 1382 (1989)
63. Seino et al., in *16th European Conf. Optical Communication, ECOC'90, Amsterdam, 1990*, p. 999
64. Macario J et al. *Opt. Express* **20** 23623 (2012)
65. Bulmer C H, Burns W K, Hiser S C *Appl. Phys. Lett.* **16** 1936 (1986)
66. Skeath P et al. *Appl. Phys. Lett.* **49** 1221 (1986)
67. Sawaki I et al., in *Technical Digest of Conf. on Lasers and Electro-Optics, CLEO'86, Washington, DC, 1986*, p. 46
68. Yamada S, Minakata M *Jpn. J. Appl. Phys.* **20** 733 (1981)
69. Seino M et al., in *Digest of Conf. Optical Fiber Communication, OFC'92* (Washington, DC: Optical Society of America, 1992) p. 325
70. Korotky S K, Veselka J *J. Lightwave Technol.* **14** 2687 (1987)
71. Maack D R, in *Reliability of Optical Fibers and Optical Fiber Systems* (Eds D K Paul, B Javidi) (Washington, DC: SPIE Optical Engineering Press, 1999) p. 197
72. Nagata H *IEEE Photon. Technol. Lett.* **12** 1477 (2000)
73. Kawanishi T, Sakamoto T, Izutsu M *J. Selected Topics Quantum Electron.* **13** 79 (2007)
74. Sano A et al., in *Technical Digest of 35th European Conf. on Optical Communication, ECOC'09, Vienna, 2009*, p. 1
75. Fujitsu Optical Components Co., Ltd. Optical Devices, https://www.fujitsu.com/jp/group/foc/en/products/devices/indexgig5.html
76. Rusing M et al. *IEEE Nanotechnol. Mag.* 18 (2019)
77. Wang C et al. *Opt. Express* **26** 1547 (2018)
78. Wang C et al. *Nature* **562** 101 (2018)
79. Loncar M, in *Technical Digest of Conf. on Lasers and Electro-Optics CLEO'2019, San Jose, CA, USA, 2019*, p. 1
80. Chelma D S et al. *Appl. Phys. Lett.* **42** 864 (1983)
81. Weiner J S, Miller D A B, Chelma D S *Appl. Phys. Lett.* **50** 842 (1987)
82. Jaques M et al. *Opt. Express* **26** 22471 (2018)
83. Joudawlkis P W et al. *Proc. SPIE* **5435** 53 (2004)
84. Kimerling L C et al. *Proc. SPIE* **6125** 612502 (2006)
85. Soref R A, Bennett B *IEEE J. Quantum Electron.* **23** 123 (1987)
86. Jalai B et al. *IEEE J. Selelected Top. Quantum Electron.* **12** 412 (2006)
87. Reed G et al. *Nat. Photon.* **4** 518 (2010)
88. Witzens J *Proc. IEEE* **106** 2158 (2018)
89. Soref R, Larenzo J *IEEE J. Quantum Electron.* **22** 873 (1986)
90. Nedelikovich M, Soref R, Mashanovich G Z *IEEE Photon. J.* **3** 1171 (2011)
91. Spector S J et al. *IEEE J. Selected Topics Quantum Electron.* **16** 165 (2010)
92. Kaminov I P et al. *J. Appl. Phys.* **51** 4379 (1980)
93. Fukano H et al. *J. Lightwave Technol.* **24** 2219 (2006)
94. Yu P K L et al., in *Intern. Topical Meeting Microwave Photonics'2005 Digest* (Piscataway, NJ: IEEE, 2005) p. 21
95. Betts G E et al. *IEEE Photon. Technol. Lett.* **18** 2065 (2006)
96. Born M, Wolf E *Principles of Optics* (Oxford: Pergamon Press, 1968); Translated into Russian: *Osnovy Optiki* (Moscow: Nauka, 1973)
97. Martin W E *Appl. Phys. Lett.* **26** 562 (1975)
98. Kissa K M et al. *J. Lightwave Technol.* **13** 1521 (1995)
99. Kawanishi T, Sakamoto T, Izutsu M *IEEE J. Selected Topics Quantum Electron.* **13** 79 (2007)
100. Izutsu M, Shikama S, Sueta T *IEEE J. Quantum Electron.* **17** 2225 (1981)
101. Griffin R A, Carter A C, in *Technical Digest of Optical Fiber Communication Conf.'2002* (Washington, DC: OSA 2002) p. 367
102. Zhou X, Yu J *J. Lightwave Technol.* **27** 3641 (2009)
103. Betts G E, in *RF Photonic Technology in Optical Fiber Links* (Ed. W S C Chang) (Cambridge: Cambridge Univ. Press, 2002) p. 81
104. Tazawa H et al. *J. Lightwave Technol.* **24** 3514 (2006)

105. Shamrai A V et al. *Quantum Electron.* **35** 734 (2005); *Kvantovaya Elektron.* **35** 734 (2005)
106. Shamrai A V et al. *Quantum Electron.* **38** 273 (2008); *Kvantovaya Elektron.* **38** 273 (2008)
107. Lebedev V V et al. *Tech. Phys. Lett.* **41** 1083 (2015); *Pis'ma Zh. Tekh. Fiz.* **41** 32 (2015)
108. Adams D, Aboketaf A, Prebe S *Opt. Express* **20** 17440 (2012)
109. Wang T et al. *J. Lightwave Technol.* **38** 1851 (2020)
110. Pandey A, Jeyasean V, Kumar S *Opt. Commun.* **461** 125224 (2020)
111. Heebner J E et al. *IEEE J. Quantum Electron.* **40** 726 (2004)
112. Bogaerts W et al. *Laser Photon. Rev.* **6** 47 (2012)
113. Zhang L et al. *IEEE J. Selected Topics Quantum Electron.* **16** 149 (2010)
114. Dumon P et al. *IEEE Photon. Technol. Lett.* **16** 1328 (2004)
115. Yariv A *IEEE Photon. Technol. Lett.* **14** 483 (2002)
116. Sacher W D *Opt. Express* **16** 15741 (2008)
117. Sacher W D et al. *Opt. Express* **21** 9722 (2013)
118. Kodanev A *IEEE Photon. Technol. Lett.* **26** 1522 (2014)
119. Hong J et al. *Sci. Rep.* **7** 4682 (2017)
120. Yang R *Opt. Express* **23** 28993 (2015)
121. Lipson M *IEEE J. Selected Topics Quantum Electron.* **12** 1520 (2006)
122. Krahenbuhl R, Howerton M M *J. Lightwave Technol.* **19** 1287 (2001)
123. Betts G E, Johnson L M, Cox C H *J. Lightwave Technol.* **7** 2078 (1989)
124. Reed G *Nat. Photon.* **4** 518 (2010)
125. Chen L *Opt. Express* **21** 27003 (2013)
126. Savchenkov A et al. *Phys. Rev. A* **76** 051804 (2004)
127. Padmaraju K, Bergman K *Nanophotonics* **3** 269 (2014)
128. Kokobun Y, Funato M, Takizava M *IEEE Photon. Technol. Lett.* **5** 1297 (1993)
129. Guha B, Kyotoku B, Lipson M *Opt. Express* **18** 3487 (2010)
130. Teng J et al. *Opt. Express* **17** 14627 (2009)
131. Djordjievich S et al. *Opt. Express* **21** 13958 (2013)
132. Dong P et al. *Opt. Express* **18** 9852 (2010)
133. Zortman W et al. *IEEE Micro* **33** 42 (2013)
134. Gheorma I L, Osgood R M *IEEE Photon. Technol. Lett.* **14** 795 (2002)
135. Petrov M P et al. *Tech. Phys. Lett.* **30** 120 (2004); *Pis'ma Zh. Tekh. Fiz.* **30** 75 (2004)
136. Arora P et al. *Opt. Commun.* **281** 2067 (2008)
137. Noriega U D et al. *Appl. Phys. B* **106** 51 (2012)
138. Greshnov A A, Lebedev V V, Shamrai A V *Tech. Phys.* **57** 1219 (2012); *Zh. Tekh. Fiz.* **82** (9) 39 (2012)
139. Alferness R C *IEEE Trans. Microwave Theory Tech.* **30** 1121 (1982)
140. Kogelnik H, Schmidt R V *IEEE J. Quantum Electron.* **12** 396 (1976)
141. Watson J E et al. *J. Lightwave Technol.* **8** 794 (1990)
142. Donelly J P, Gopinath A A *IEEE J. Quantum Electron.* **23** 30 (1987)
143. Tsuzuki K et al. *Electron. Lett.* **39** 1464 (2003)
144. Kuz'minov Yu S *Niobat i Tantalat Litiya. Materialy dlya Nelineinoi Optiki* (Lithium Niobate and Tantalate. Materials for Nonlinear Optics) (Moscow: Nauka, 1975)
145. Lebedev V V et al. *Tech. Phys. Lett.* **40** 743 (2014); *Pis'ma Zh. Tekh. Fiz.* **40** (17) 39 (2014)
146. Noguchi K *J. Opt. Fiber Commun.* **4** 1 (2007)
147. Wang C et al. *Nature* **562** 101 (2018)
148. Petrov V M et al. *Fotonika* (5) 414 (2020)
149. Enami Y et al. *Nat. Photon.* **1** 180 (2007)
150. Varlamov A V et al. *Tech. Phys. Lett.* **43** 994 (2017); *Pisma Zh. Tekh. Fiz.* **43** (21) 87 (2017)
151. Wong K K (Ed.) *Properties of Lithium Niobate* (London: INSPEC, 2002)
152. Wang X et al. *APL Photon.* **4** 096101 (2019)
153. Macario J et al. *Opt. Express* **20** 23623 (2012)
154. Gopalakrishnan G K, Burns W K, Bulmer C H *Electron. Lett.* **28** 207 (1992)
155. Shi Y *IEEE Trans. Microwave Theory Tech.* **54** 810 (2006)
156. Kondo J et al. *IEEE Photon. Technol. Lett.* **17** 2077 (2005)
157. Fukuma M, Noda J *Appl. Opt.* **19** 591 (1980)
158. Alferness R C, Buhl L L, Divino M D *Electron. Lett.* **18** 490 (1982)
159. Ramaswamy V, Alferness R C, Divino M *Electron. Lett.* **18** 30 (1982)
160. Borghesani A, in *Optical Fiber Communication Conf., Technical Digest* (Washington, DC: Optical Society of America, 2003) paper ThO1
161. Delansay P et al. *Electron. Lett.* **32** 1820 (1996)
162. Kim H, Gnauk A H *IEEE Photon. Technol. Lett.* **14** 298 (2002)
163. Tronev A et al. *J. Phys. Conf. Ser.* **951** 012002 (2018)
164. Lu P et al. *Appl. Phys. Rev.* **6** 041302 (2019)
165. Yamaguchi V Y et al. *Jpn. J. Appl. Phys.* **53** 08MB03 (2014)
166. Tronev A et al. *Proc. SPIE* **10535** 1053527 (2018)
167. Koyama F, Iga K *J. Lightwave Technol.* **6** 87 (1988)
168. Laverdiere C, Fekecs A, Tetu M *IEEE Photon. Technol. Lett.* **15** 446 (2003)
169. Gnauk A H et al. *IEEE Photon. Technol. Lett.* **3** 916 (1991)
170. Catherle J C *J. Lightwave Technol.* **16** 372 (1998)
171. Ackerman E, Microwave Theory Tech. IEEE Trans. 47.2271-2279.10.1109/22.808970 (2000)
172. Fereira A et al., in *Technical Digest 11-th Intern. Conf. on Transparent Optical Networks, Azores, 2009*, p. 1
173. https://www.infinera.com/wp-content/uploads/The-Advantages-of-InP-Photonic-Integration-in-High-Performance-Coherent-Optics-0223-WP-RevA-1219.pdf
174. Doerr C R *Frontiers Phys.* **3** 37 (2015)
175. Cheng Q et al. *Optica* **5** 1354 (2018)
176. Shen Y et al. *J. Lightwave Technol.* **37** 245 (2019)
177. Alibart O et al. *J. Opt.* **18** 104001 (2016)
178. Lonchar M, in *Technical Digest of 2019 Conf. on Lasers and Electro-Optics, San Jose, CA, USA, 2019*, p. 1
179. Rusing M et al. *IEEE Nanotechnol. Mag.* **13** 18 (2019)